



THESIS

STUDY OF SIDELobe REDUCTION ON FRACTAL-BASED CONFORMAL ARRAYS USING GENETIC ALGORITHM

SONGKRAN PISANUPOJ

**GRADUATE SCHOOL, KASETSART UNIVERSITY
2008**



THESIS APPROVAL
GRADUATE SCHOOL, KASETSART UNIVERSITY

Master of Engineering (Electrical Engineering)

DEGREE

Electrical Engineering

FIELD

Electrical Engineering

DEPARTMENT

TITLE: Study of Sidelobe Reduction on Fractal-based Conformal Arrays Using Genetic Algorithm

NAME: Mr. Songkran Pisanupoj

THIS THESIS HAS BEEN ACCEPTED BY

THESIS ADVISOR

(Associate Professor Nuttaka Homsup, Ph.D.)

COMMITTEE MEMBER

(Assistant Professor Waroth Kuhirun, Ph.D.)

COMMITTEE MEMBER

(Mrs. Jantane Rungrangpitayagon, Ph.D.)

DEPARTMENT HEAD

(Associate Professor Mongkol Raksapatcharawon, Ph.D.)

APPROVED BY THE GRADUATE SCHOOL ON _____

DEAN

(Associate Professor Gunjana Theeragool, D.Agr)

THESIS

STUDY OF SIDELobe REDUCTION ON FRACTAL-BASED CONFORMAL ARRAYS USING GENETIC ALGORITHM

SONGKRAN PISANUPOJ

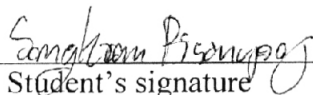
A Thesis Submitted in Partial Fulfillment of
the Requirements for the Degree of
Master of Engineering (Electrical Engineering)
Graduate School, Kasetsart University

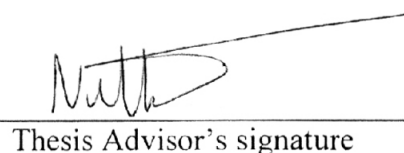
2008

Songkran Pisanupoj 2008: Study of Sidelobe Reduction on Fractal-based Conformal Arrays Using Genetic Algorithm. Master of Engineering (Electrical Engineering), Major Field: Electrical Engineering, Department of Electrical Engineering. Thesis Advisor: Associate Professor Nuttaka Homsup, Ph.D. 72 pages.

The conformal antennas, which normally fitted to non-flat surface such as vehicle or airplane exterior structure, have one of the major problems is high sidelobe level. In this study, we generate the antenna array models by using fractal geometry, the Peano-gosper curve, to strategically place elements of the arrays. Then we project initial arrays to 3 selected surfaces to form 3 conformal arrays. This research proposes the analysis of the fractal array behavior in sidelobe reduction when conformed to various surfaces.

We set up the experiment on these arrays to evaluate the sidelobe reduction by using genetic algorithm concept optimization, performing on the array factor of each models. Our results show that genetic algorithm has a good capability to decrease sidelobe level of our models. The array factor sidelobe level is reduced at minimum -13 dB from nearly zero. Another setting model shows that current excitation may have a little effect on the performance of the genetic algorithm in sidelobe level decline. One major factor that affects the sidelobe reduction is the shape of conformed surface. The outcome of each different mounted surfaces shows that the capability in sidelobe reduction has a few effect from current excitation.


Student's signature


Thesis Advisor's signature

3 / 6 / 2008

ACCKNOWLEDGEMENT

The author would like to thank Associate Professor Nuttaka Homsup for her advice and assistance, in adjusting and correcting the contents and for serving as her major advisor. The author is deeply grateful for Assistant Professor Waroth Kuhirun who gave useful suggestions for this research. The author wishes to express his appreciation to Mr. Meta Polpasee for his kindly support in giving useful suggestions. Finally, I would like to dedicate all my works to my family who encourages me and gives me a chance to experience in the world of living and learning.

Songkran Pisanupoj

May 2008

TABLE OF CONTENTS

	Page
TABLE OF CONTENTS	i
LIST OF TABLES	ii
LIST OF FIGURES	iii
INTRODUCTION	1
LITERATURE REVIEW	2
MATERIAL AND METHOD	21
Materials	21
Methods	21
RESULTS AND DISCUSSION	24
Results	24
Discussion	48
CONCLUSION AND RECOMMENDATION	65
Conclusion	65
Recommendation	65
LITERATURE CITED	66
CURRICULUM VITAE	72

LIST OF TABLES

Table		Page
1	Comparison planar array and conformal array	7
2	Example initial population	18
3	Example selected population after 50% selection rate	19
4	General Parameters of the simulation model	24
5	Summarized Result of the experiments	51

LIST OF FIGURES

Figure	Page
1 Polar power pattern of isotropic source	2
2 (a) Power pattern and (b) relative power pattern for same source. Both patterns have the same shape. The relative power pattern is normalized to a maximum of unity (1).	3
3 The pattern in (a) three-dimensional, (b) polar and (c) decibel display with the polarity of the lobes alternate (+ and -).	5
4 Linear plot of power pattern and its associated lobes.	9
5 Koch snowflake at several stages of growth (a) initiator, (b) stage 1, (c) stage 2, (d) stage 3	12
6 Sierpinski carpet at several stages of growth (a) stage 1, (b) stage 2, (c) stage 3, (d) stage 4	13
7 The Peano-gosper initiator	14
8 The Peano-gosper curve generator	14
9 The first three stages in the construction of self-avoiding Peano-Gosper curve. The stage 1 is shown as the dashed line superimposed on the stage 1 generator. The generator (unscaled) is shown again in (b) as the dashed curve superimposed on the stage 2 Peano-gosper curve	15
10 Flowchart of genetic algorithm	17
11 Example of mating	19
12 Example of mutated chromosomes	20
13 Flow chart of methodologies	22
14 Element locations for the (a) x-z, (b) y-z, and (c) x-y views of x-axis cylindrical conformed array.	24
15 3-dimension view of conformed array with printed number of elements.	26

LIST OF FIGURES (continued)

Figure		Page
16	Evolution diagram of genetically optimized conformed array shows the reduction of sidelobe level from nearly zero to -12.497dB.	26
17	Normalized genetically optimized array factor versus (a) θ for $\varphi = 90^\circ$, (b) φ for $\theta = 90^\circ$ and (c) top view of the radiation pattern of the x-axis cylindrical conformal array	27
18	Element locations for the (a) x-z, (b) y-z, and (c) x-y views of y-axis cylindrical conformed array	29
19	3-dimension view of y-axis cylindrical conformed array with printed number of elements.	31
20	Evolution diagram of genetically optimized conformed array shows the reduction of sidelobe level from zero to -13.179 dB.	31
21	Normalized genetically optimized array factor versus (a) θ for $\varphi = 90^\circ$, (b) φ for $\theta = 90^\circ$ and (c) top view of the radiation pattern of the y-axis cylindrical conformal array.	32
22	Element locations for the (a) x-z, (b) y-z, and (c) x-y views of cosine-ring conformed array	34
23	3-dimension view of conformed array.	36
24	Evolution diagram of genetically optimized conformed array shows the reduction of sidelobe level from -3.5 to -7.168dB.	36
25	Normalized genetically optimized array factor versus (a) θ for $\varphi = 90^\circ$, (b) φ for $\theta = 90^\circ$ and (c) top view of the radiation pattern of the cosine-ring conformal array.	37
26	Evolution diagram of genetically optimized conformed array shows the reduction of sidelobe level from about -2 dB to -12.223 dB.	39

LIST OF FIGURES (continued)

Figure		Page
27	Normalized genetically optimized array factor versus (a) θ for $\varphi = 90^\circ$, (b) φ for $\theta = 90^\circ$, and (c) top view of the radiation pattern of the x-axis cylindrical conformal array.	40
28	Evolution diagram of genetically optimized conformed array shows the reduction of sidelobe level from about -1 dB to -12.093 dB.	42
29	Normalized genetically optimized array factor versus (a) θ for $\varphi = 90^\circ$, (b) φ for $\theta = 90^\circ$, and (c) top view of the radiation pattern of the y-axis cylindrical conformal array.	43
30	Evolution diagram of genetically optimized conformed array shows the reduction of sidelobe level from about -3.7 dB to -9.193 dB.	45
31	Normalized genetically optimized array factor versus (a) θ for $\varphi = 90^\circ$, (b) φ for $\theta = 90^\circ$, and (c) top view of the radiation pattern of the cosine-ring conformal array.	47
32	Evolution diagrams show the comparison of the sidelobe level for each models between current excitation maximum (I_{max}) equal to 5 (solid line) and 1 (dash line) (a) x-axis cylindrical conformal array, (b) y-axis cylindrical conformal array and (c) cosine-ring surface conformal array.	50
33	Evolution diagram shows comparison of sidelobe level between each models for (a) the maximum current excitation equal to 5 and (b) the maximum current excitation equal to 1, solid line as x-axis cylindrical, dash-dot line as y-axis cylindrical and dash line as cosine-ring.	51
34	Radiation pattern of 2000 th generation x-cylindrical conformal array that the maximum current excitation equals to 5 at different sizes of minimum spacing (d_{min}): (a) $\lambda/2$, (b) $3\lambda/4$ and (c) λ .	53

LIST OF FIGURES (continued)

Figure		Page
35	Radiation pattern of 2000 th generation x-cylindrical conformal array that the maximum current excitation equals to 1 at different sizes of minimum spacing (d_{min}): (a) $\lambda/2$, (b) $3\lambda/4$, and (c) λ .	55
36	Radiation pattern of 2000 th generation y-cylindrical conformal array that the maximum current excitation equals to 5 at different sizes of minimum spacing (d_{min}): (a) $\lambda/2$, (b) $3\lambda/4$, and (c) λ .	57
37	Radiation pattern of 2000 th generation y-cylindrical conformal array that the maximum current excitation equals to 1 at different sizes of minimum spacing (d_{min}): (a) $\lambda/2$, (b) $3\lambda/4$, and (c) λ .	59
38	Radiation pattern of 2000 th generation cosine-ring conformal array that the maximum current excitation equals to 5 at different sizes of minimum spacing (d_{min}): (a) $\lambda/2$, (b) $3\lambda/4$, and (c) λ .	61
39	Radiation pattern of 2000 th generation cosine-ring conformal array that the maximum current excitation equals to 1 at different sizes of minimum spacing (d_{min}): (a) $\lambda/2$, (b) $3\lambda/4$, and (c) λ .	63

STUDY OF SIDELobe REDUCTION ON FRACTAL-BASED CONFORMAL ARRAYS USING GENETIC ALGORITHM

INTRODUCTION

Analysis and design of antenna arrays synthesizing with a main beam and sidelobes have been of interest for amount of time. The implementations of those antennas are various used on many surfaces which are not just flat planar. Many that have been fitted to non-flat surface, such as vehicle or airborne exterior structure, are conformal antennas. Conformal array antennas are normally expected to be use to mobile communication or radars. In such application, one of the major problems is how to provide antennas with low sidelobe to avoid electromagnetic interference.

Recently, Fractal geometry has been applied to numerous designs of antenna arrays with the improvement in sidelobe reduction and broadband coverage. More over, the concept of fractal gives the self-similar characteristic and space-filling capability. Various fractal geometries have been observed such as Koch curves, Sierpinski curves, Peano curves, and so on which are widely employed in many applications.

In this study, the objective is to analyze the fractal array behavior in sidelobe reduction when conformed to various surfaces. We use genetic algorithm (GA) to determine the sidelobe level through the vast space of solution. GA is an optimization method based on the theory of natural selection which is suitable for a large number of parameters like excitation on each element of fractal arrays.

LITERATURE REVIEW

1. Isotropic point source

1.1 Definition of isotropic point source

An isotropic point source is a source that radiates energy uniformly in all directions. For such a source the radial component S_r of the Poynting vector is independent of θ and Φ . A graph of S_r at a constant radius as a function of angle is a Poynting vector, or power-density, pattern, but is usually called power pattern. The three-dimensional power pattern for an isotropic source is a sphere. In two dimensions the pattern is a circle, as in Figure 1

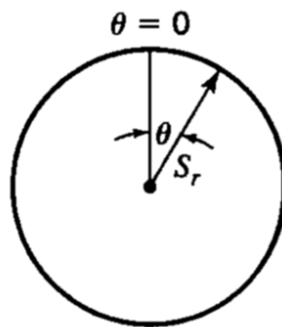


Figure 1 Polar power pattern of isotropic source

The isotropic source is not a physically realizable type. Even the simplest antennas have directional properties. As an example the power pattern of such a source is shown in Figure 2 where S_{rm} is the maximum value of S_r .

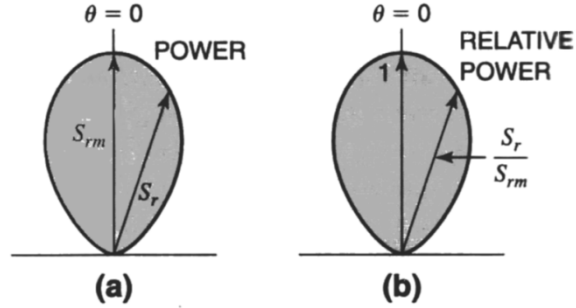


Figure 2 (a) Power pattern and (b) relative power pattern for same source. Both patterns have the same shape. The relative power pattern is normalized to a maximum of unity (1). (Kraus and Marhefka, 2003)

S_r can be expressed in 3 different ways, *absolute power pattern*, *relative power pattern* and *normalized pattern*. *Absolute power pattern* is expressed in watt per square meter. If S_r is expressed in terms of its value in some reference direction, the graph is a *relative power pattern*. Thus, the pattern radius for relative power is S_r/S_{rm} where S_{rm} is the maximum value of S_r . A pattern with a maximum of unity is called a *normalized pattern*.

1.2 Field patterns

Since the power from a point source has only a radial component which can be considered as a scalar quantity. For point sources we deal with far fields so E and H are entirely transverse to the wave direction, perpendicular to each other, in-phase, and related in magnitude by intrinsic impedance of medium ($E/H=Z=377\Omega$ for free space). Thus, the Poynting vector around a point source is everywhere radial, the electric field is entirely transverse, having only E_θ and E_ϕ component. The conditions characterizing the far field are:

- Poynting vector radial (S_r component only)
- Electric field transverse (E_θ and E_ϕ component only)

At a point of far field the Poynting vector and the electric field are related as they are in plane wave, if r is sufficiently large. The relation between the average Poynting vector and the electric field is

$$S_r = \frac{1}{2} \frac{E^2}{Z}$$

Where Z_0 = intrinsic impedance of medium and

$$E = \sqrt{E_\theta^2 + E_\phi^2}$$

Where E = amplitude of total electric field intensity

E_θ = amplitude of θ component

E_ϕ = amplitude of ϕ component

A pattern showing variation of the electric field intensity at a constant radius r as a function of angle (θ, ϕ) is called a *field pattern*. The magnitudes of both the electric field components of the far field vary inversely as the distance from the source. However, they may be different functions, F_1 and F_2 , of the angular coordinates, θ and ϕ .

1.3 Phase pattern

If the field varies harmonically with time and the frequency is known, the far field in all directions from a source may be specified by four quantities:

- 1) Amplitude of the polar component E_θ of the electric field as a function of r , θ , and ϕ
- 2) Amplitude of the azimuthal component E_ϕ of the electric field as a function of r , θ , and ϕ

- 3) Phase lag δ of E_ϕ behind E_θ as a function of θ and ϕ
- 4) Phase lag η of either field component behind its value at a reference point as a function of r , θ , and ϕ

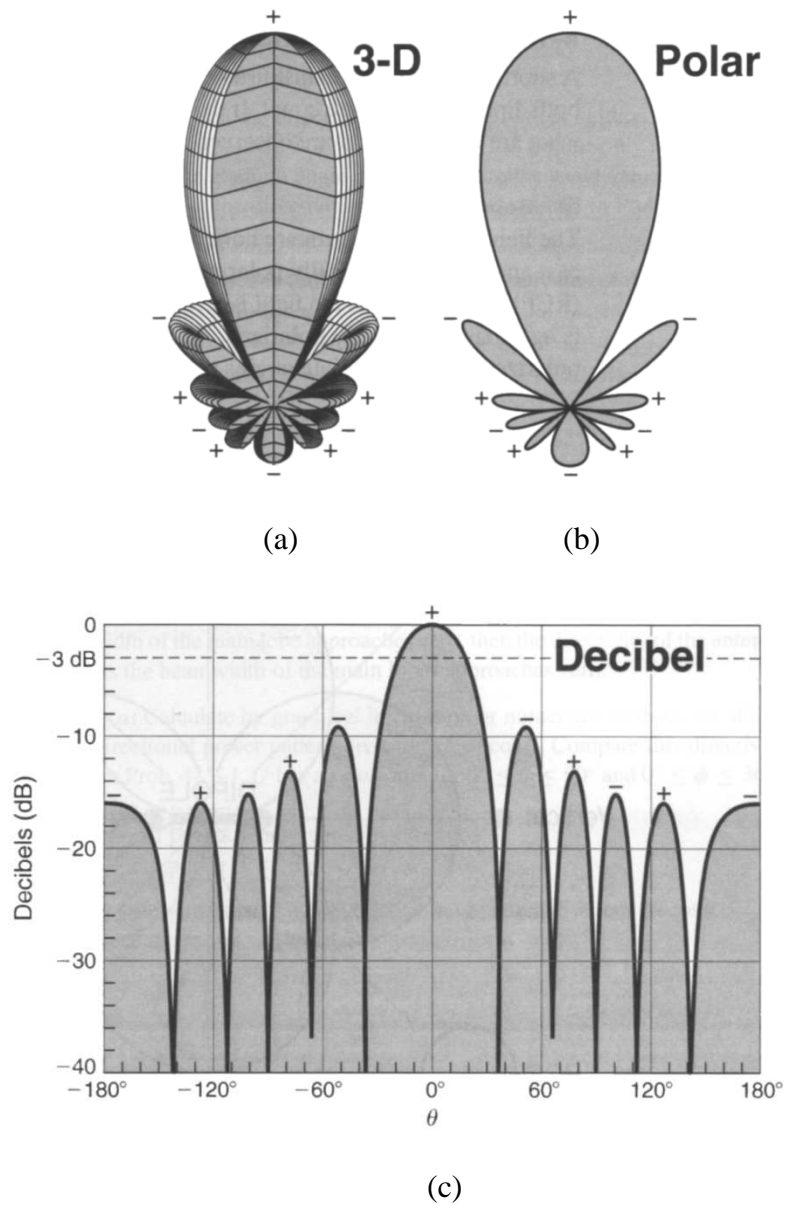


Figure 3 The pattern in (a) three-dimensional, (b) polar and (c) decibel display with the polarity of the lobes alternate (+ and -). (Kraus and Marhefka, 2003)

2. Conformal array

2.1 Definition of a conformal antenna

A conformal antenna is an antenna that conforms to something. The shape can be some part of an airplane, high-speed train, or other vehicle. The purpose is to build the antenna so that it becomes integrated with the structure and does not cause extra drag. The purpose can also be that the antenna integration makes the antenna less disturbing, less visible to the human eye; for instance, in an urban environment. A typical additional requirement in modern defense systems is that the antenna not backscatter microwave radiation when illuminated by, for example, an enemy radar transmitter (i.e., it has stealth properties).

The IEEE Standard Definition of Terms for Antennas (IEEE Std 145-1993) gives the following definition:

2.74 Conformal antenna [conformal array]. An antenna [an array] that conforms to a surface whose shape is determined by considerations other than electromagnetic; for example, aerodynamic or hydrodynamic.

2.75 Conformal array. See: conformal antenna.

2.2 Why conformal?

Many conformal antennas have been used on a modern aircraft. There can be more than 20 different antennas for a commercial airplane and up to 70 for militaries, such number may causing considerable drag and increase fuel consumption. The integration of antennas to the aircraft skin is highly recommended. Some of the antenna functions should be combined in the same unit if the design can be made broadband enough. The need for conformal antennas is more for the large-sized apertures that are necessary for communications. (i.e., satellites and radars)

Table 1 Comparison planar array and conformal array

Parameter	Planar array	Conformal array
Technology	Mature	Not fully established
Analysis tools	Available	In development
Beam control	Phase only usually sufficient, fixed amplitude	Amplitude and phase, more complicated
Polarization	Single can be used (dual often desired)	Polarization control required, especially if doubly curved
Gain	Drops with increased scan	Controlled, depends on shape
Frequency bandwidth	Typically 20%	Wider than planar is possible
Angular coverage	Limited to roughly $\pm 60^\circ$	Very wide, half sphere
Radar Cross Section	Large specular RCS	Lower than planar

3. Array factor, main lobe and side lobe

3.1 Array factor

Consider an N -element antenna array located in three-dimensional space. Suppose that the n^{th} element of the 3-D array is located at the rectangular coordinate (x_n, y_n, z_n) . Suppose that the n^{th} element of the array n^{th} has current amplitude excitation I_n and relative phase β_n . In terms of the position vector \vec{r}_n , the array factor of this 3-D antenna array can be expressed as:

$$AF(\hat{n}) = \sum_{n=1}^N I_n \exp[j(k\hat{r}_n \cdot \hat{n} + \beta_n)] \quad (3.1)$$

where \hat{n} is a unit vector in direction of field point.

In this study, we set the relative phase to zero ($\beta_n = 0$) and the direction of mainlobe to z-axis so that θ_0 and φ_0 are zero. The array factor of an N -element antenna array in 3-D space is given by

$$\begin{aligned} AF(\theta, \varphi) &= AF(\vec{\Psi}) = \sum_{n=1}^N I_n \exp(j\vec{r}_n \cdot \vec{\Psi}) \\ &= \sum_{n=1}^N I_n \exp(j(\Psi_x x_n + \Psi_y y_n + \Psi_z z_n)) = AF(\Psi_x, \Psi_y, \Psi_z) \\ &= AF(\vec{n}) = \sum_{n=1}^N I_n \exp(jk\vec{r}_n \cdot \hat{n}) \\ &= \sum_{n=1}^N I_n \exp(jk(n_x x_n + n_y y_n + n_z z_n)) = AF(n_x, n_y, n_z) \end{aligned} \quad (3.2)$$

where $\vec{\Psi}$ is a vector whose component in the x-, y- and z-axes are Ψ_x , Ψ_y and Ψ_z respectively, and \vec{n} is a unit vector whose components along the x-, y- and z-axes are n_x , n_y and n_z respectively

$$AF(\vec{\Psi}) = AF(\hat{n}) = \sum_{n=1}^N I_n e^{(j\vec{r}_n \cdot \vec{\Psi})} = AF(\hat{n}) = \sum_{n=1}^N I_n e^{(j\vec{n} \cdot \hat{n})} \quad (3.3)$$

The function has the following properties:

1. The visible region is $|\hat{n}_x + \hat{n}_y + \hat{n}_z| \leq |\hat{n}| = 1$ or $|\bar{\Psi}_x + \bar{\Psi}_y + \bar{\Psi}_z| \leq |\bar{\Psi}| = k$

2. The visible region of the function

$$AF(\bar{\Psi} - \bar{\Psi}_0) = AF(\hat{n} - \hat{n}_0) = \sum_{n=1}^N I_n e^{(j\vec{r} \cdot \langle \bar{\Psi} - \bar{\Psi}_0 \rangle)} = AF(\hat{n}) = \sum_{n=1}^N I_n e^{(jk\vec{r}_n \cdot \langle \bar{n} - \bar{n}_0 \rangle)}$$

$$\text{is } \left| (\hat{n}_x - \hat{n}_{x_0}) + (\hat{n}_y - \hat{n}_{y_0}) + (\hat{n}_z - \hat{n}_{z_0}) \right| \leq |\hat{n} - \hat{n}_0| = 1 \text{ or}$$

$$\left| (\bar{\Psi}_x - \bar{\Psi}_{x_0}) + (\bar{\Psi}_y - \bar{\Psi}_{y_0}) + (\bar{\Psi}_z - \bar{\Psi}_{z_0}) \right| \leq |\bar{\Psi}| = k$$

3. $AF(\bar{\Psi}) = \overline{AF(-\bar{\Psi})}$ and $AF(\hat{n}) = \overline{AF(-\hat{n})}$

4. $AF_1(a\hat{n}) = AF_2(\hat{n})$ where a is a scalar quantity and $AF_1(\hat{n})$ and $AF_2(\hat{n})$ are the arrays factors in term of \hat{n} with the minimum spacing $d_{\min} = d_1$ and $d_2 = ad_1$, respectively.

3.2 The mainlobe and sidelobes

According to the beampattern in Figure 4, the highest peak in the mainlobe while the smaller peaks are Sidelobe. The beampattern may be interpreted as the spatial filter response of an array. Thus the mainline is similar to the passband in a spatial band-pass filter, which only passes signals in these directions. Similar to filter design in digital signal processing, we would like the beam to approach the delta pulse or equally an infinitely thin beam. But from array processing theory, this is impossible using an array with finite spatial extension. The location of mainlobe peak tells in which direction we get maximum response with the array. Another measure used to characterize the mainlobe is the mainlobe width or the beamwidth. Here we define it to be the full width of the mainlobe at 6dB below the mainlobe peak on the beampattern from the angular array pattern; we can measure at which angle 2ϕ the mainlobe has dropped 6dB.

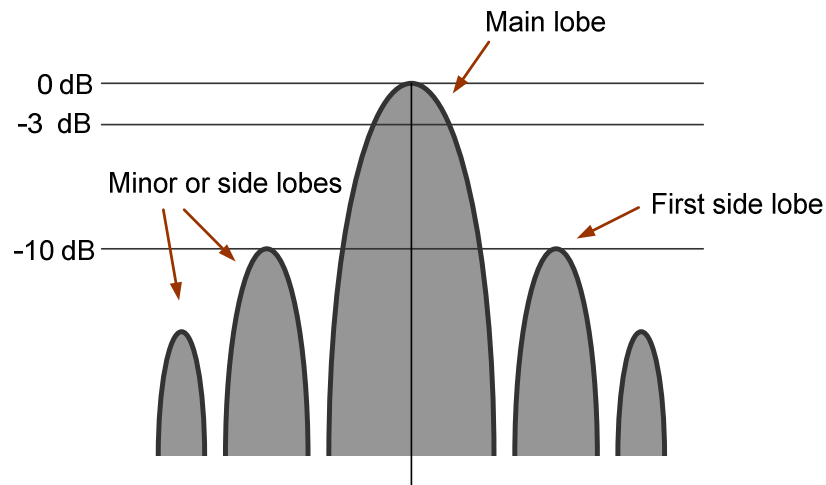


Figure 4 Linear plot of power pattern and its associated lobes.

The beamwidth is then ϕ for consistency and usually measured in degrees. The Sidelobe in the beampattern is equal to the stopband in a bandpass filter. As is known from window filter design, the Sidelobe can not be completely rejected using a finite aperture. But the Sidelobe can be suppressed a certain degree by adjusting the amplitude weights and elements positions. The sidelobe region or equally the stopband, is conveniently defined as the area in the plane outside the first zero crossing of the mainlobe. The sidelobe level is used as a measure on the height of the highest sidelobe peak in the sidelobe region and usually given in decibel (dB). The height of the highest sidelobe relative to the mainlobe measures an array's ability to reject unwanted noise and signals, and focus on particular propagating signals.

4. Fractal geometry

4.1 Background of Fractal

A fractal is generally "a rough or fragmented geometric shape that can be subdivided into parts, each of which is (at least approximately) a reduced-size copy of the whole," a property called self-similarity. The term was coined by Benoît Mandelbrot in 1975 and was derived from the Latin "fractus" meaning "broken" or "fractured". Mathematicians who played major role in developing the fractals are, for example, Cantor (1872), Peano (1890), Hilbert (1891), Koch (1904), Sierpinski (1916), Julia (1918). Originally, the fractal geometry was used to describe complex shapes in nature that cannot be easily characterized by Euclidean geometry. A fractal often has the following characteristics:

- A fine structure at arbitrarily small scales.
- Too irregular to be easily described in traditional Euclidean geometric language.
- Self-similarity (at least approximately or stochastically).
- A Hausdorff dimension which is greater than its topological dimension (although this requirement is not met by space-filling curves such as the Hilbert curve).
- A simple and recursive definition.

4.2 Examples of Fractal

Fractals are normally generated by recursive processes of dilations and translations of an initial set. Each of fractals has its own initial set or generator that shapes in elementary form but can produce a complex form of fractal.

a) Koch Snowflake

Start with an equilateral triangle and replace the middle third of every line segment with a pair of line segments that form an equilateral "bump." Then perform the same replacement on every line segment of the resulting shape, ad infinitum. Every iterations, the perimeter of this shape grows by $1/3^{\text{rd}}$. The Koch snowflake is the result of an infinite number of these iterations, and has an infinite length, while its area remains finite.

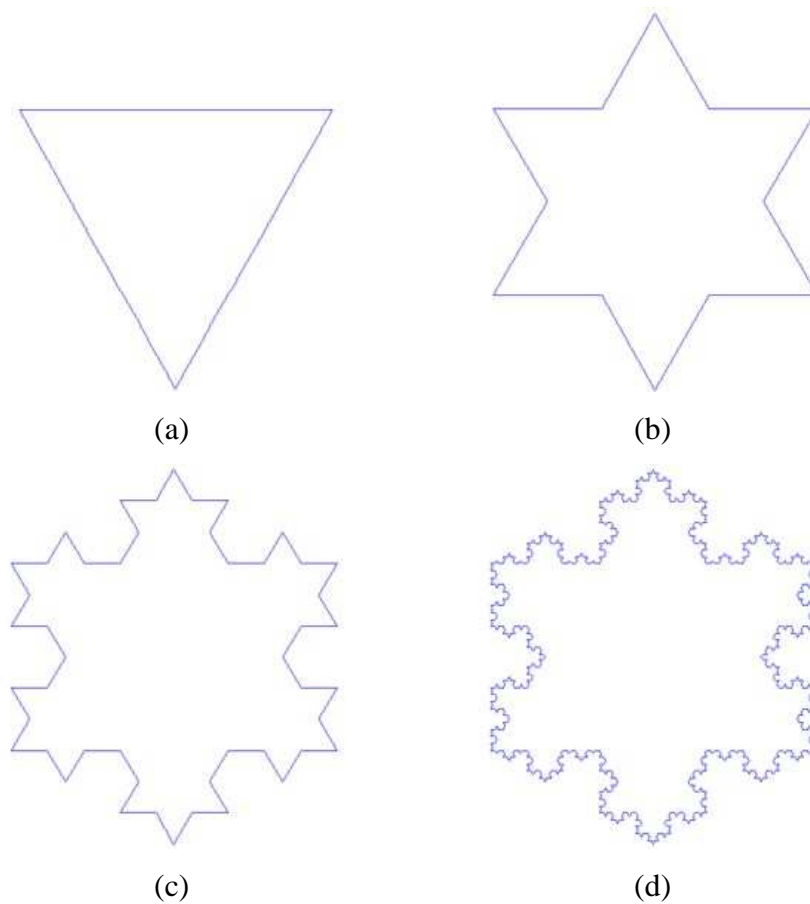


Figure 5 Koch snowflake at several stages of growth (a) initiator, (b) 1st stage, (c) 2nd stage, (d) 3rd stage.

b) Sierpinski carpet

The construction of the Sierpinski carpet begins with a square. The square is cut into 9 congruent subsquares in a 3-by-3 grid, and the central subsquare is removed. The same procedure is then applied recursively to the remaining 8 subsquares for an infinite time. So we obtain the Sierpinski carpet.

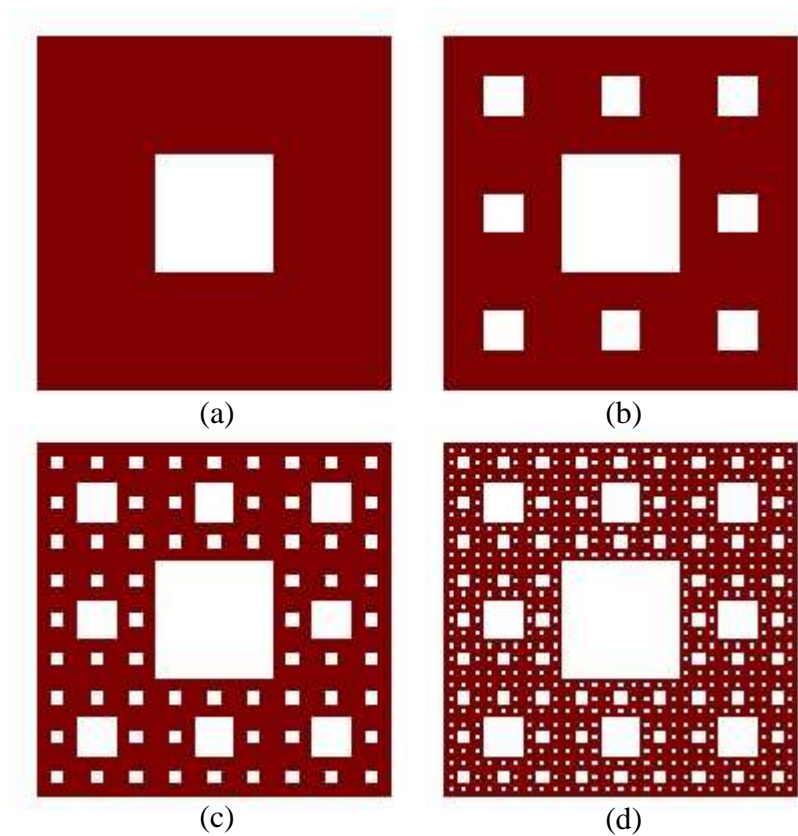


Figure 6 Sierpinski carpet at several stages of growth (a) 1st stage (b) 2nd stage (c) 3rd stage (d) 4th stage.

c) Peano-gosper curve

The forming procedure of Peano-gosper curve starts with a straight line of 1 unit as an initiator. Then replace the initiator with Peano-gosper curve generator for stage 1. Stage 2; turn the generator counterclockwise until the link between both ends is aligned in the same direction as of each line segment of the generator(s) in the previous stage. Scale the generator to the same size as that of each line segment of generator and replace each of previous stage lines with an appropriate scaled of the generator.

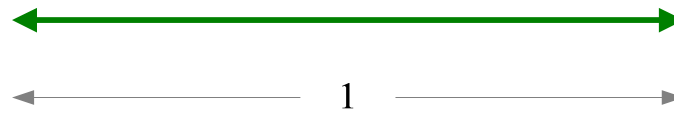


Figure 7 The Peano-gosper initiator

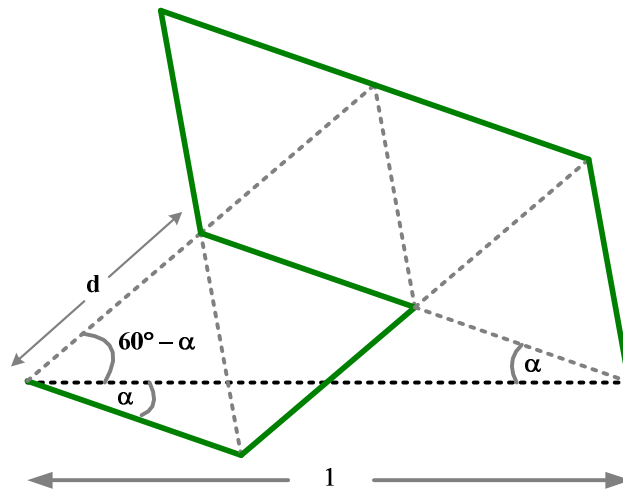


Figure 8 The Peano-gosper curve generator

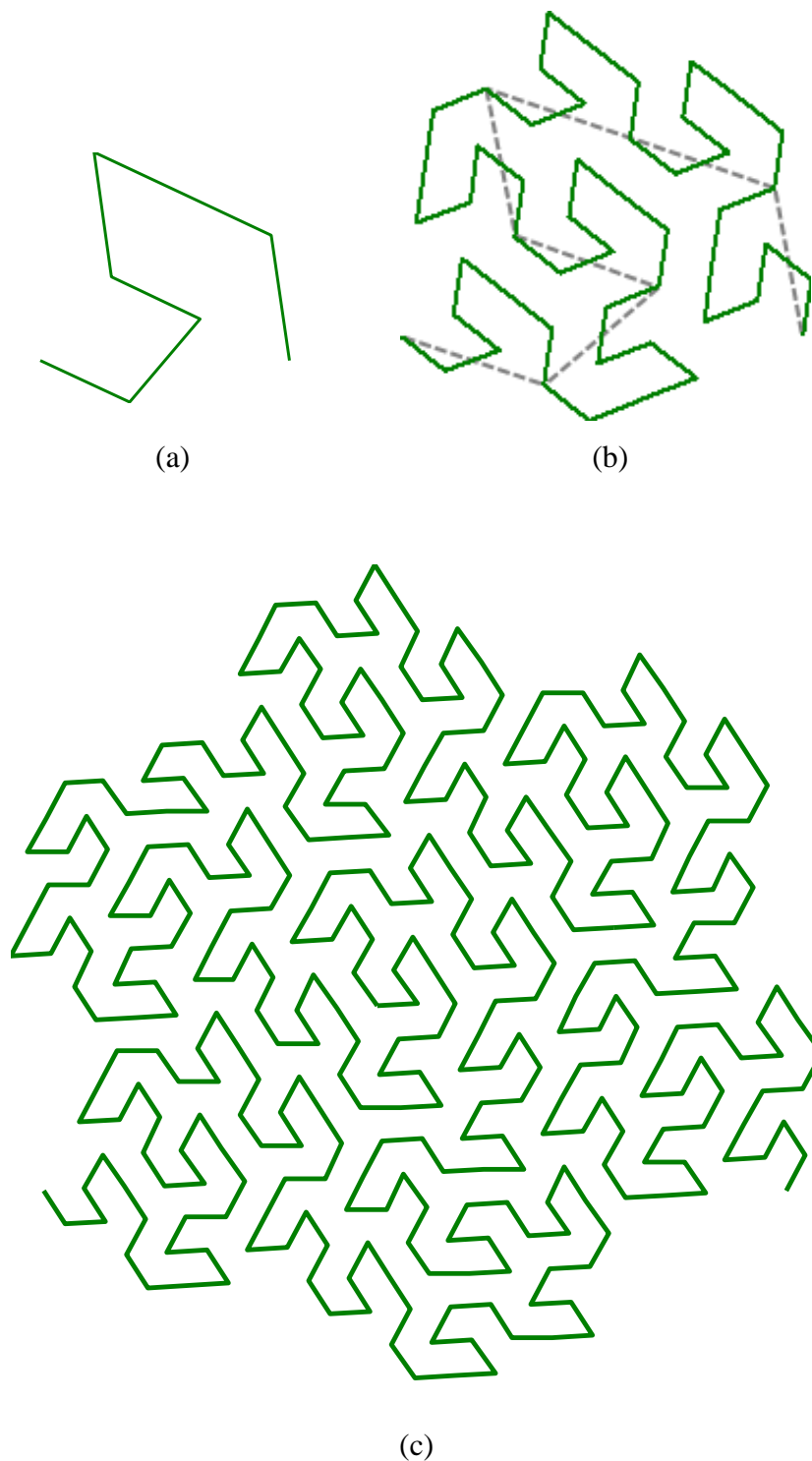


Figure 9 The first three stages in the construction of self-avoiding Peano-Gosper curve. The stage 1 is shown as the dashed line superimposed on the stage 2 generator. The generator (unscaled) is shown again in (b) as the dashed curve superimposed on the stage 2 Peano-gosper curve

5. Genetic algorithm

5.1 Overview

Genetic algorithm (GA) is an optimization and search technique based on the principles of genetics and natural selection. A GA allows a population composed of many individuals to evolve under specified selection rules to a state that maximizes the “fitness”. GA has some advantages that it

- Optimizes with continuous or discrete variables,
- Doesn't require derivative information,
- Simultaneously searches form a wide sampling of the cost surface,
- Deals with a large number of variables,
- Is well suited for parallel computers,
- Optimizes variable with extremely complex cost surface (they can jump out a local minimum),
- Provide a list of optimum variable, not just a single solution,
- May encode the variable so that optimization is done with the encoded variable
- Work with numerically generated data , experimental data, or analytical function

Even GA is intriguing and produces stunning results, but GA is not the best way to solve every problem.

5.2 Component of a Genetic algorithm

GA begins, like any other optimization algorithm, by defining the optimization variables, the cost function, and the cost. It ends like other optimization algorithms too, by testing for convergence. In between this algorithm has some different. A path through the components of the GA is shown as an overview flowchart in Figure 10.

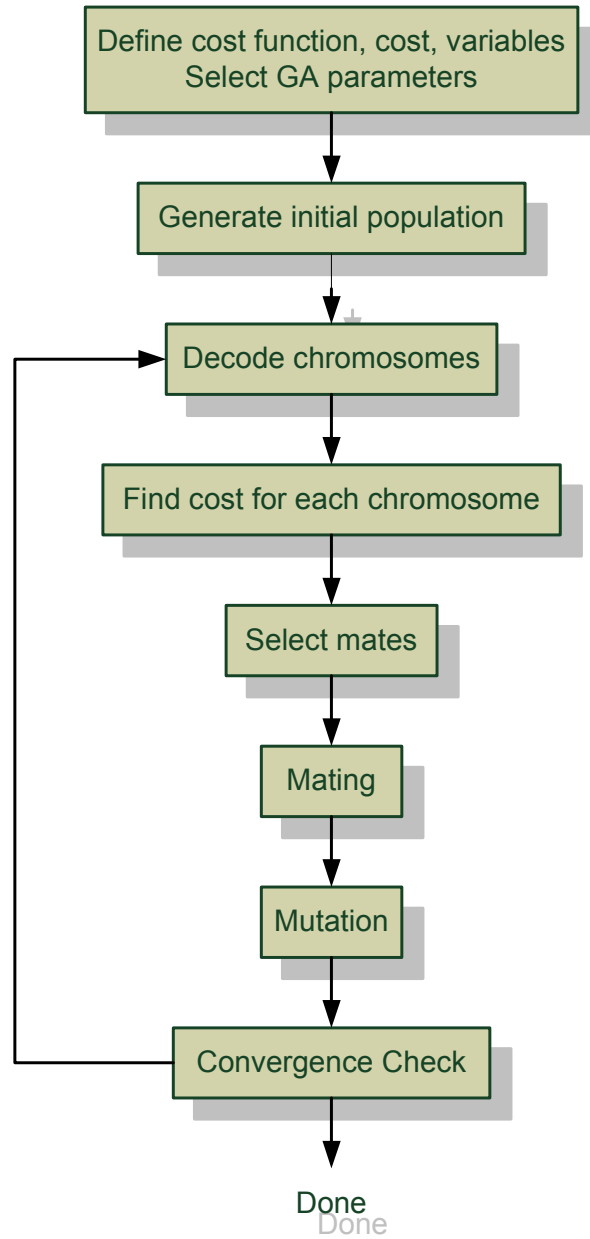


Figure 10 Flowchart of genetic algorithm

The GA begins by defining a chromosome or an array of variable values to be optimized. If the chromosome has N_{var} variables given by $p_1, p_2, \dots, p_{N_{\text{var}}}$, then the chromosome is written as an N_{var} element row vector.

$$\text{chromosome} = [p_1, p_2, \dots, p_{N_{\text{var}}}] \quad (5.1)$$

Each chromosome has a cost found by evaluating the cost function, f , at $p_1, p_2, \dots, p_{Nvar}$

$$cost = f(\text{chromosome}) = f(p_1, p_2, \dots, p_{Nvar}) \quad (5.2)$$

After everything has settled, GA starts by generating a group of chromosomes known as population. The population has N_{pop} chromosomes and is an $N_{pop} \times N_{bits}$ matrix filled with random ones and zeros generated using

$$pop = \text{round}(\text{rand}(N_{pop}, N_{bits}));$$

Table 2 Example initial population

Chromosome												Cost
0	1	1	0	1	0	1	0	1	0	0	1	-98
1	1	0	0	0	1	0	1	0	0	0	0	-134
1	0	0	0	0	0	1	1	0	0	1	0	-123
0	1	1	0	1	0	1	0	0	0	0	1	-113
0	0	1	0	1	1	1	0	0	0	0	1	-125
1	1	1	0	0	0	0	1	1	0	1	0	-110

The selection of fittest population is to discard the chromosomes with highest cost. First, the N_{pop} costs and associated chromosomes are ranked from lowest to highest. Then, only the best are selected to continue with the selection rate, X_{rate} , which is the fraction of N_{pop} that survives for next step. The number of chromosomes that kept each generation is

$$N_{keep} = X_{rate} N_{pop} \quad (5.3)$$

Table 3 Example selected population after 50% selection rate

Chromosome	Cost
1 1 0 0 0 1 0 1 0 0 0 0	-134
0 0 1 0 1 1 1 0 0 0 0 1	-125
1 0 0 0 0 0 1 1 0 0 1 0	-123

Two chromosomes are selected from N_{keep} chromosomes to produce two new offspring, until $N_{pop} - N_{keep}$ offspring are born to replace the discarded chromosomes. This process is called “Mating”. The most common form of mating involves two parents that produce two offspring. A crossover point is randomly selected between the first and last bits of parents’ chromosomes. Consequently the offspring contain portion of the chromosomes of both parents.

Parent 1	1 1 0 0 0 1 0 1 0 0 0 0
Parent 2	0 0 1 0 1 1 1 0 0 0 0 1
Offspring 1	1 1 0 0 0 1 1 0 0 0 0 1
Offspring 2	0 0 1 0 1 1 0 1 0 0 0 0

Figure 11 Example of mating

Mutations will be added at the end of mating process. Random mutations alter a certain percentage of the bits in the list of chromosomes. A single point mutation changes a 1 to 0, and visa versa. Mutation points are randomly selected from the total number of bits in the population matrix. The number of mutation is given by;

$$\#mutations = \mu \times (N_{pop} - 1) \times N_{bits} \quad (5.4)$$

Where μ is mutation rate in percent

Offspring 1	1	1	0	0	0	1	1	0	0	0	0	1
Offspring 2	0	0	1	0	1	1	0	1	0	0	0	0
Mutated Offspring 1	1	1	0	0	1	1	1	0	0	0	0	1
Mutated Offspring 2	0	0	1	0	1	1	0	1	1	0	0	0

Figure 12 Example of mutated chromosomes

After the mutations take place, the costs associated with the offspring and mutated chromosomes are calculated. The process described is iterated. Then the processes are repeated, after ranking chromosomes the selection has been made and the discarded chromosomes are replaced by offspring from kept parents.

MATERIAL AND METHOD

Materials

1. Personal Computer (AMD Athlon™ XP3800 Dual Core⁺ 1.67GHz processor, 1GB DDRRAM)
2. MATLAB™ (MATrix LABoratory) version 7.5

Methods

The purpose of this research is to study the behavior of array antennas on sidelobe reduction when conformed to various surfaces. By using the concept of genetic algorithm, we search through the wide space of solutions. We start with developing Matlab codes to generate the selected conformal fractal arrays and to synthesize the arrays with low sidelobes. Then analyze results of sidelobe reduction.

1. Generating the fractal-based conformal arrays

1.1 Generate the 3rd stage Peano-gosper curve to specify the coordinates for fractal array. By using procedure mentioned above we've acquired a Peano-gosper curve at the 3rd stage. Assume that the array elements are positioned on each corner and each end of the curve, so we gain 344 array elements along the 3rd stage Peano-gosper curve.

1.2 Conform the array to selected surfaces by project each coordinate of elements to the selected surface. We have chosen several shapes of surfaces that are parabolic dome shape, part of cylindrical shape, and cosine-ring shape. So we obtain coordinates of conformed arrays.

2. Sidelobe evaluation with Genetic algorithm

This research main objective is to analyze how fractal arrays behave when conformed to surfaces. By using concept of genetic algorithm we synthesize our arrays with low sidelobe level. Several of surfaces, arrays being mounted, are presenting different sidelobe levels and patterns.

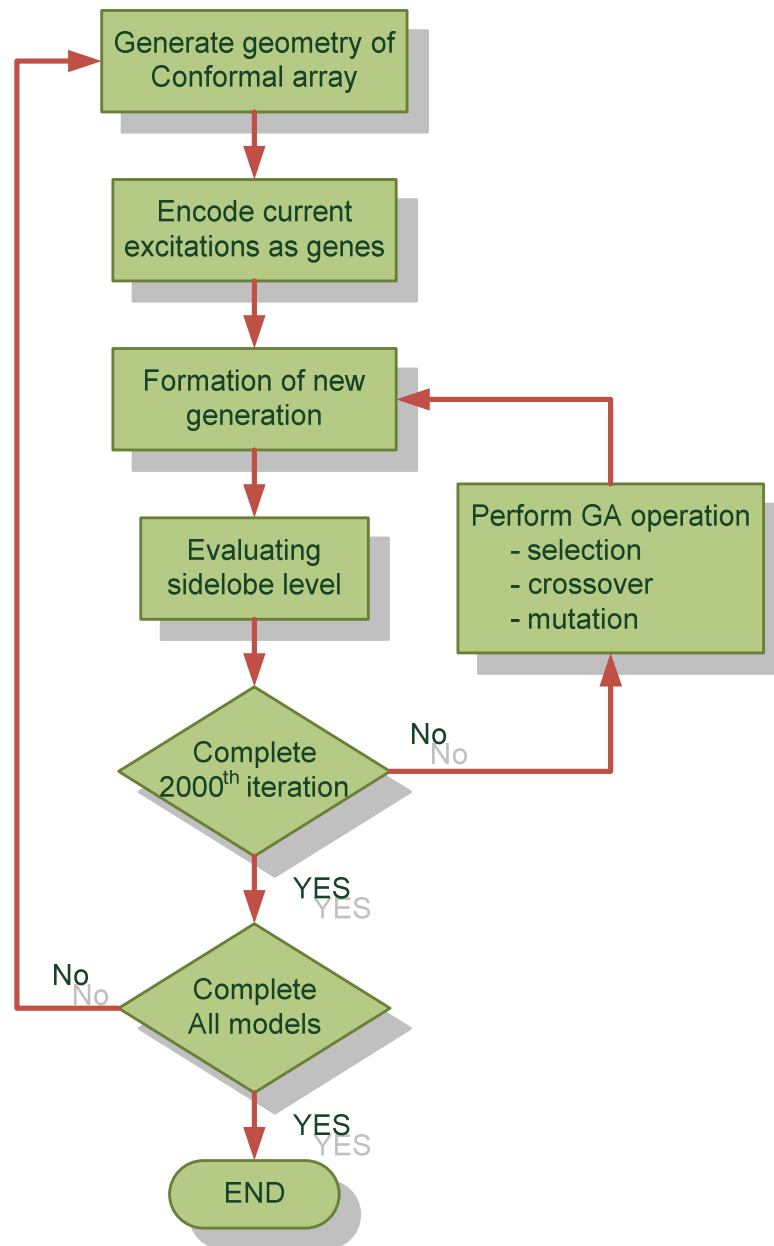


Figure 13 Flow chart of methodologies

We represent a relative current excitation on 344 elements of array by a 344-decimal gene chromosome which is used in the process of sidelobe evaluations with concept of genetic algorithm. We've generated 16 chromosomes that the genes are randomized from 0 to 5 as the initial populations. After evaluating the initial population by sidelobe level, 50 percent of fittest chromosomes are selected and the rest are discarded. The remained chromosomes are matched to produce offsprings. In the crossover process, the crossover point is determined at the middle of each chromosome. Mutation rate is set to 10 percent and a mutated gene is randomly selected from 344 genes in a chromosome. This work is aimed to run each model for 2000 iterations.

3. Analysis the results

We repeat evaluating sidelobe levels in all selected models so that there is sufficient data to analyze.

RESULTS AND DISCUSSION

Results

1. Peano-gosper conformal arrays synthesis using genetic algorithm 1st setting

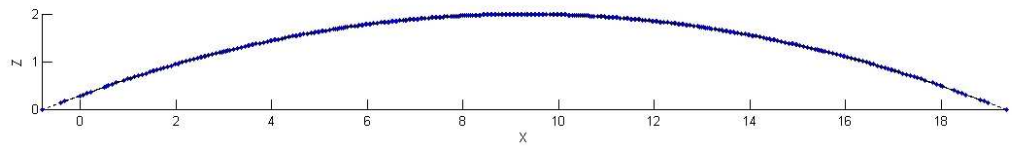
We've set up the model parameters as shown in Table 4

Table 4 General Parameters of the simulation model

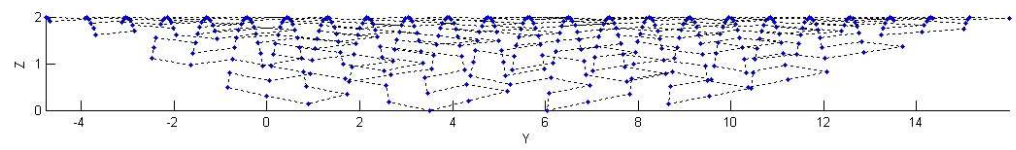
Parameter	Value
Minimum space between elements (d_{min})	λ
Peano-gosper stage of growth	3
Current excitation (I_n)	0-5
Number of chromosome in a generation	16
Number of generations in GA process	2000

1.1 Simulation results of Peano-gosper array conformed to a cylindrical surface by x-axis

By integrate each coordinate of elements of the array to a cylindrical shape with the height (Z) equal to 2 times of d_{min} we acquire the geometry of the conformed array as shown in Figure14. We used GA to optimize the sidelobe level of the array. Figure17 shows the normalized plot of array factor and Figure16 shows the reduction of sidelobe level in 2000 generation that have been performed.

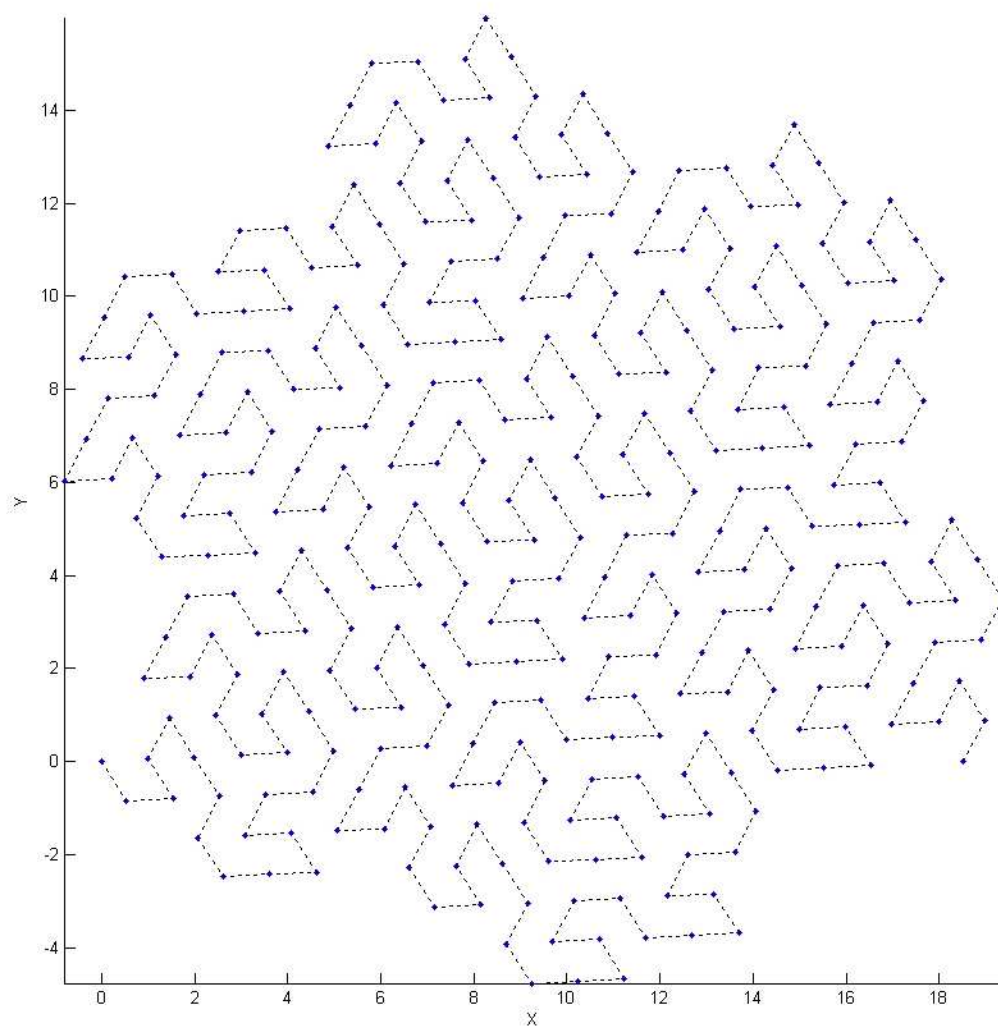


(a)



(b)

Figure 14 Element locations for the (a) x-z, (b) y-z, and (c) x-y views of x-axis cylindrical conformed array.



(c)

Figure 14 (continued)

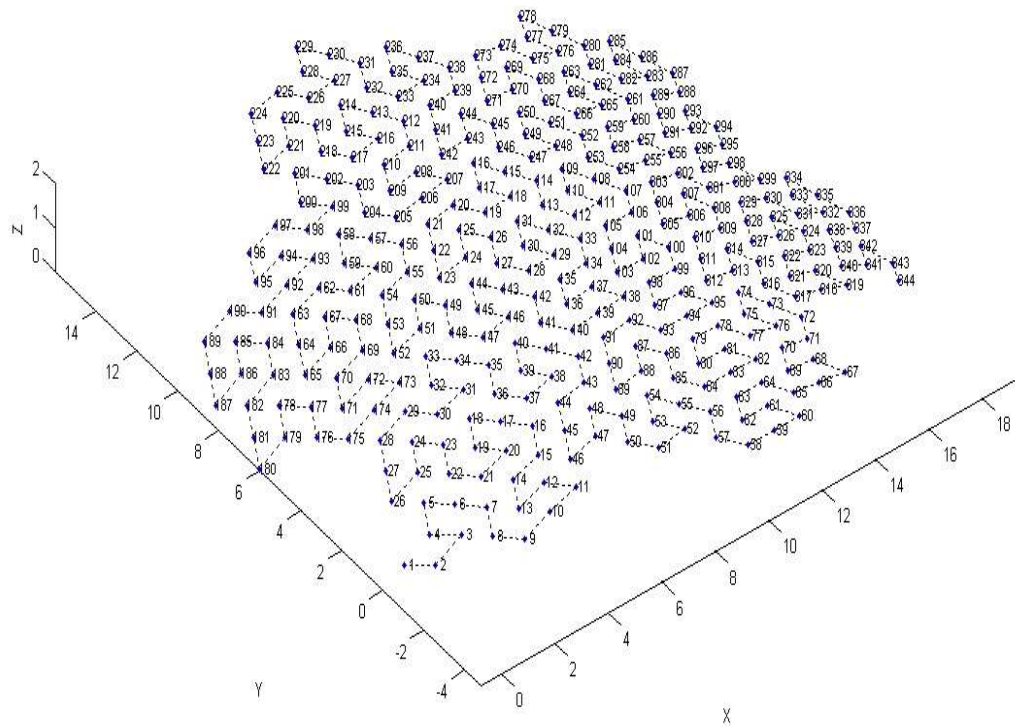


Figure 15 3-dimension view of conformed array with printed number of elements.

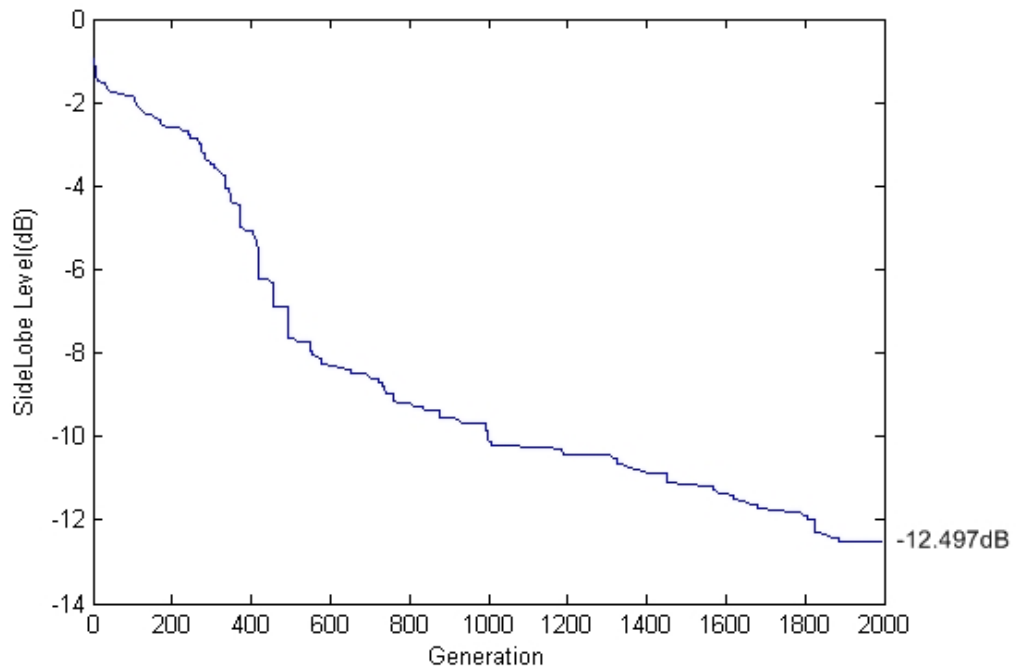
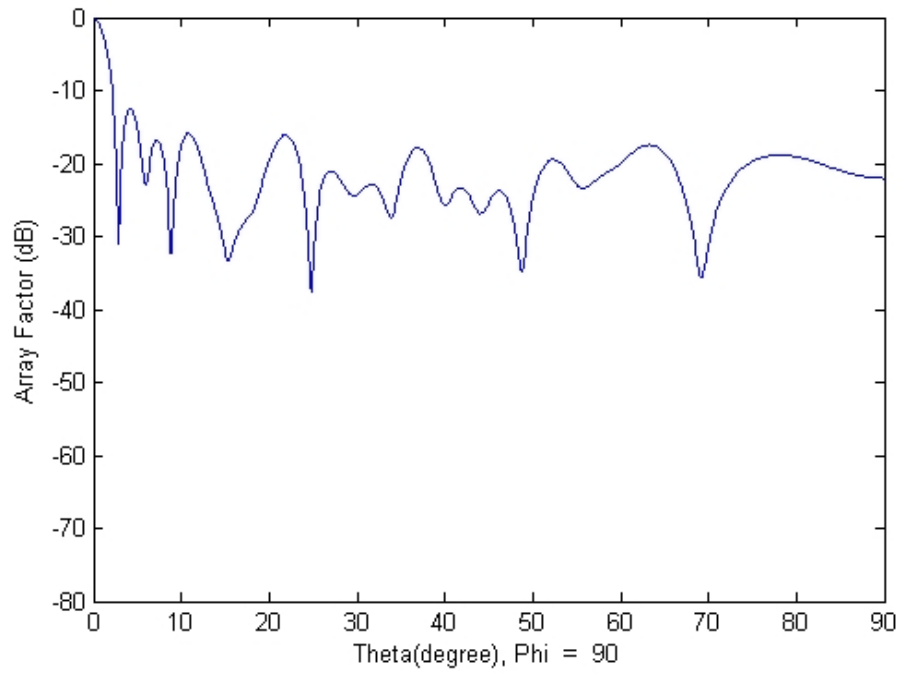
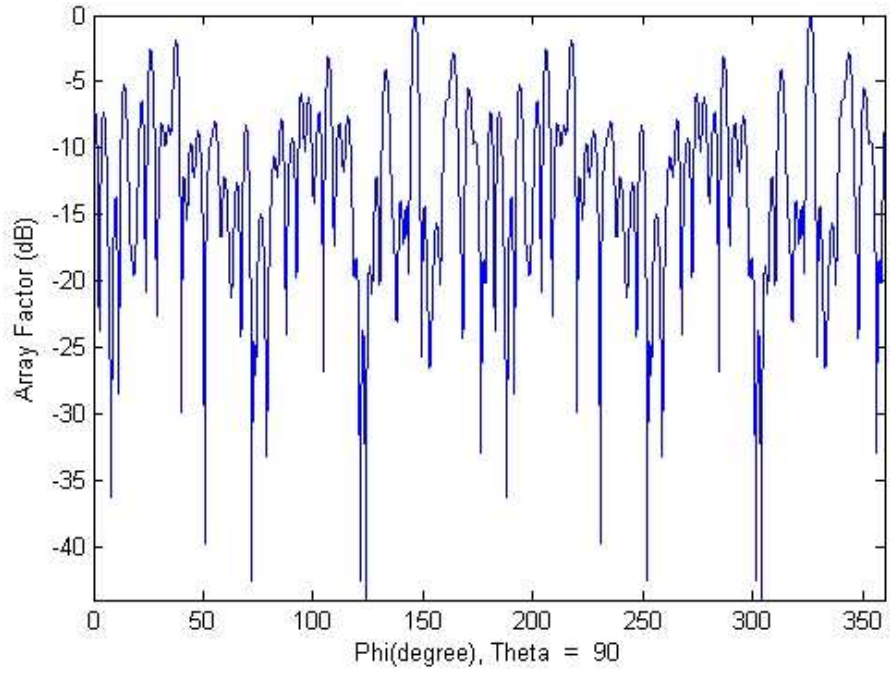


Figure 16 Evolution diagram of genetically optimized conformed array shows the reduction of sidelobe level from nearly zero to -12.497 dB.



(a)



(b)

Figure 17 Normalized genetically optimized array factor versus (a) θ for $\phi = 90^\circ$, (b) ϕ for $\theta = 90^\circ$, and (c) top view of the radiation pattern of the x-axis cylindrical conformal array.

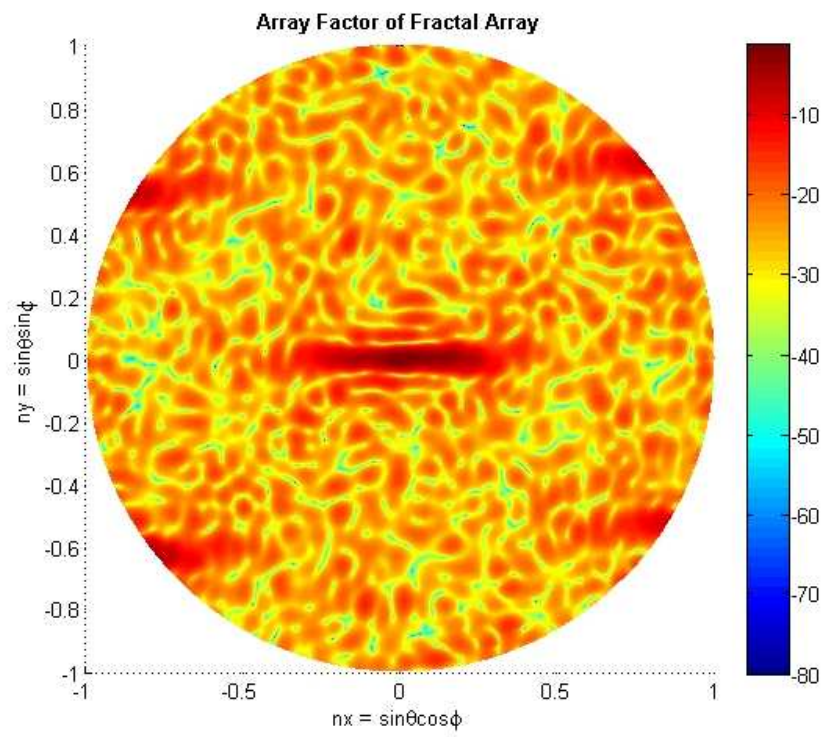
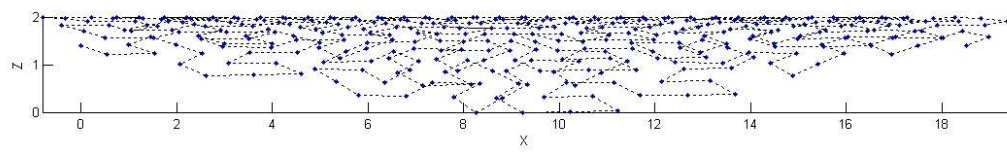


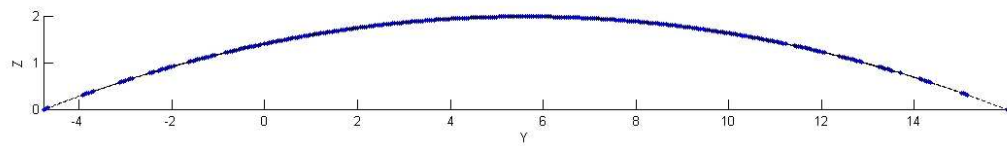
Figure 17 (continued)

1.2 Simulation results of Peano-gosper array conformed to a cylindrical surface by y-axis

We've change the axis of cylindrical shape to y-axis, other settings using the same as 1.1. We have got the result from the simulation as shown in Figure 18

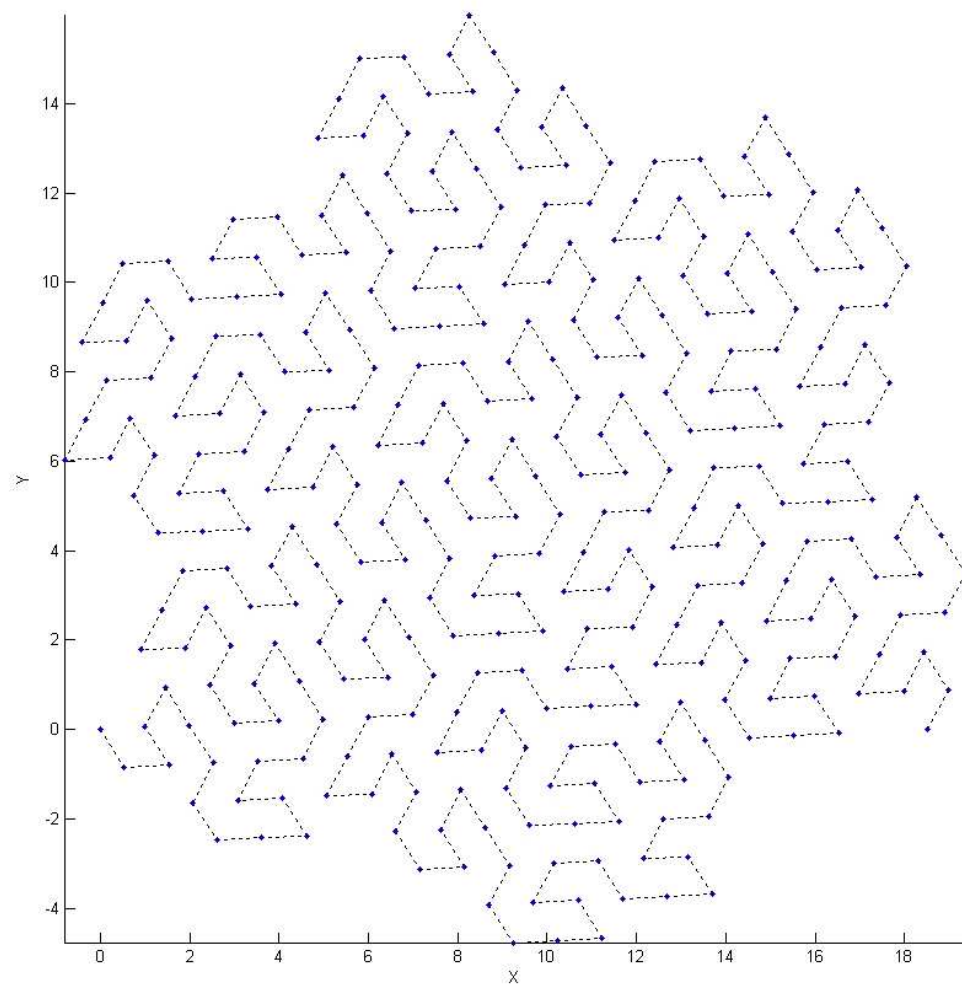


(a)



(b)

Figure 18 Element locations for the (a) x-z, (b) y-z, and (c) x-y views of y-axis cylindrical conformed array.



(c)

Figure 18 (continued)

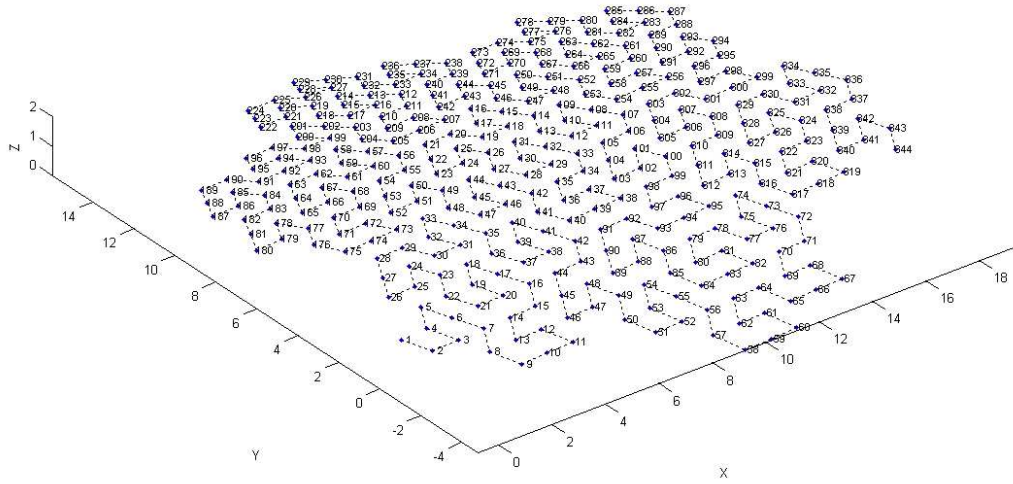


Figure 19 3-dimension view of y-axis cylindrical conformal array with printed number of elements.

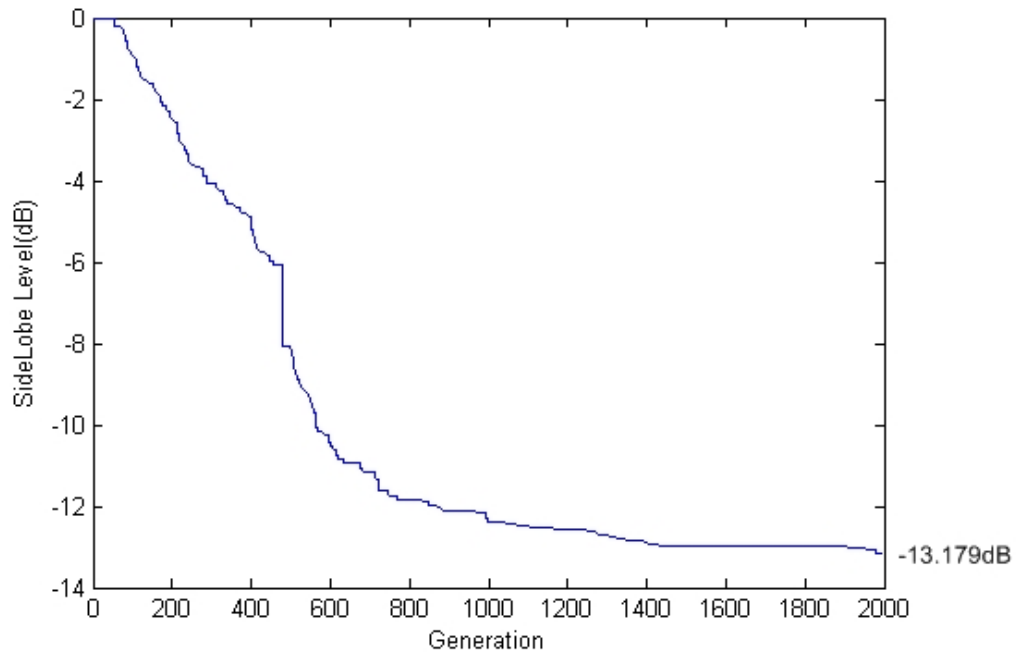
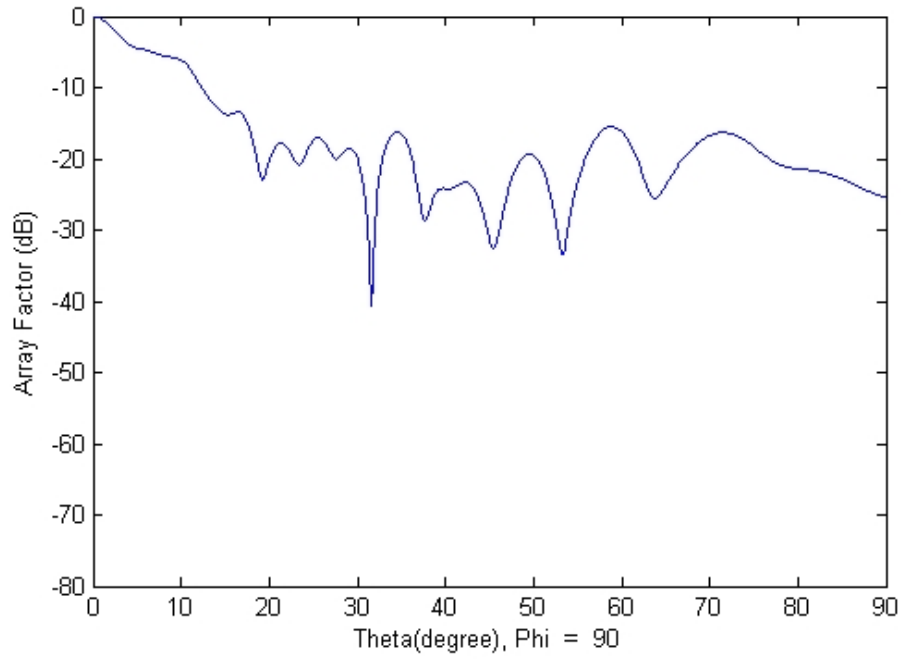
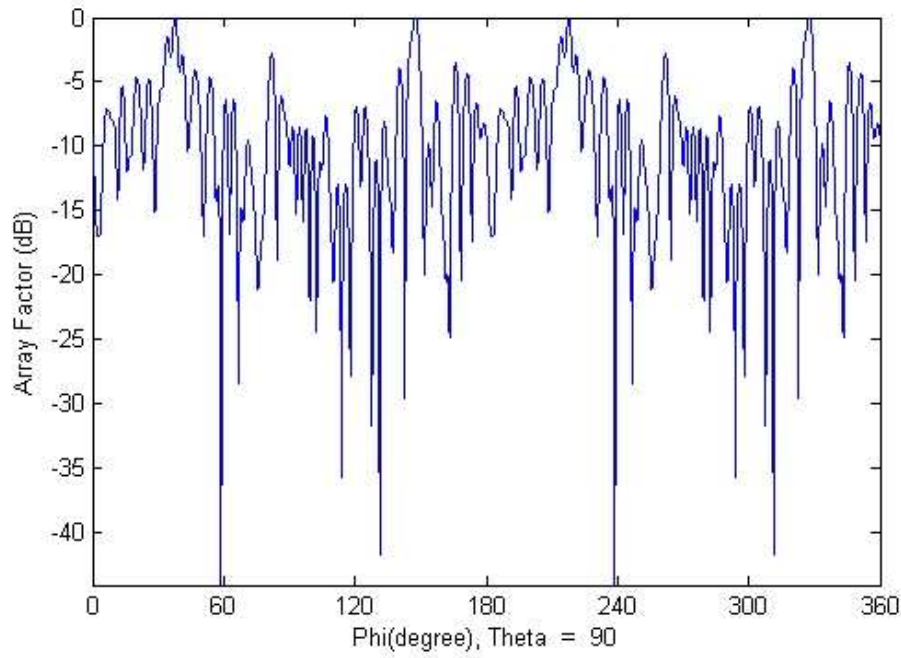


Figure 20 Evolution diagram of genetically optimized conformal array shows the reduction of sidelobe level from zero to -13.179 dB.

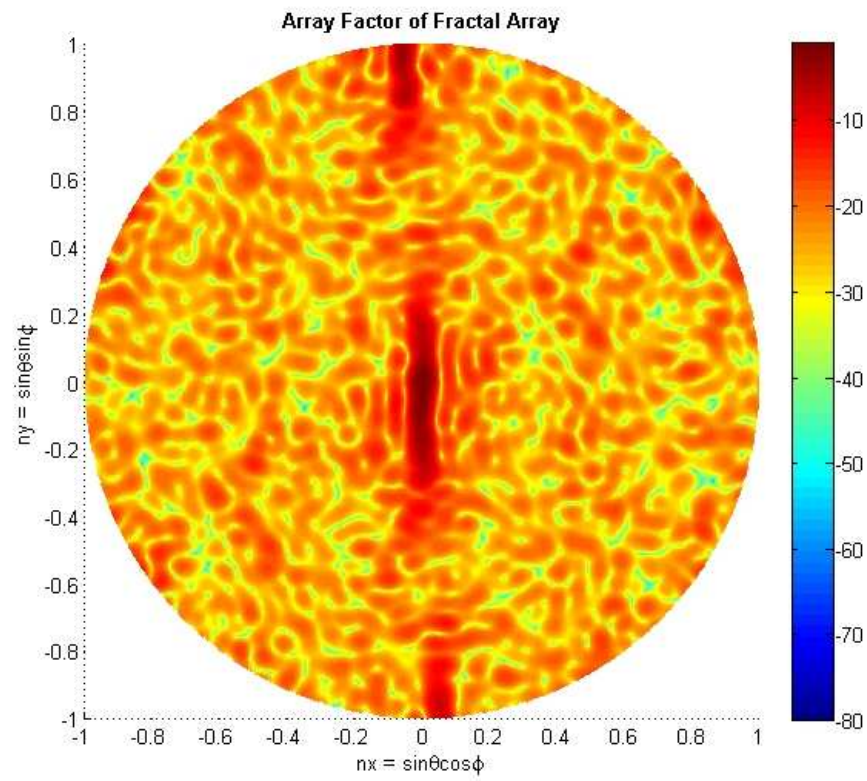


(a)



(b)

Figure 21 Normalized genetically optimized array factor versus (a) θ for $\varphi = 90^\circ$, (b) φ for $\theta = 90^\circ$, and (c) top view of the radiation pattern of the y-axis cylindrical conformal array.

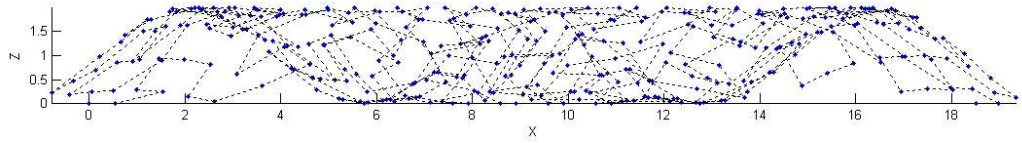


(c)

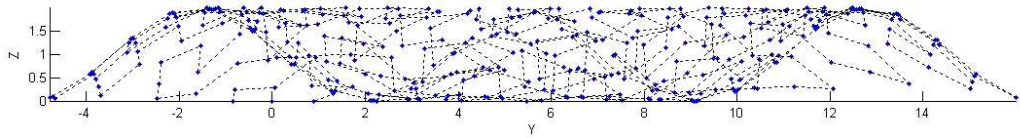
Figure 21 (continued)

1.3 Simulation results of Peano-gosper array conformed to a cosine-ring surface.

The results of Peano-gosper based conformal array that conformed to cosine-ring surface are shown as follow:

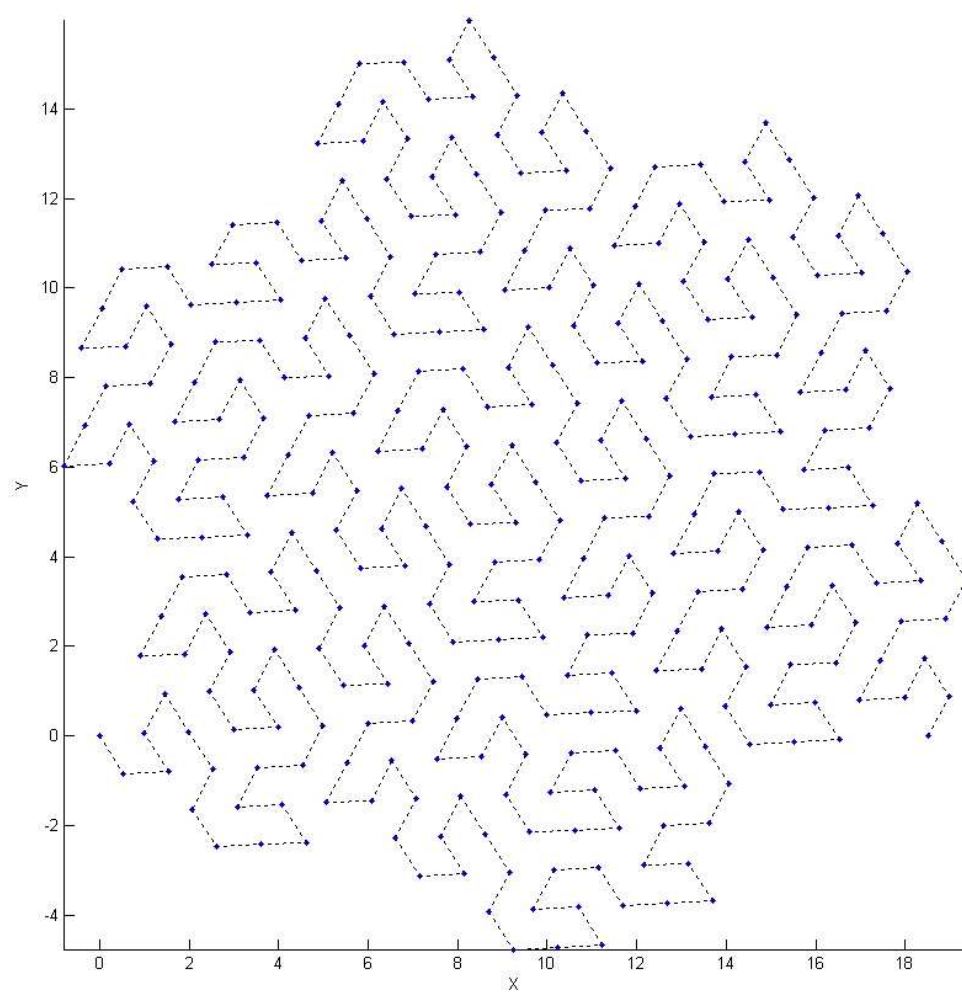


(a)



(b)

Figure 22 Element locations for the (a) x-z, (b) y-z, and (c) x-y views of cosine-ring conformed array



(c)

Figure 22 (continued)

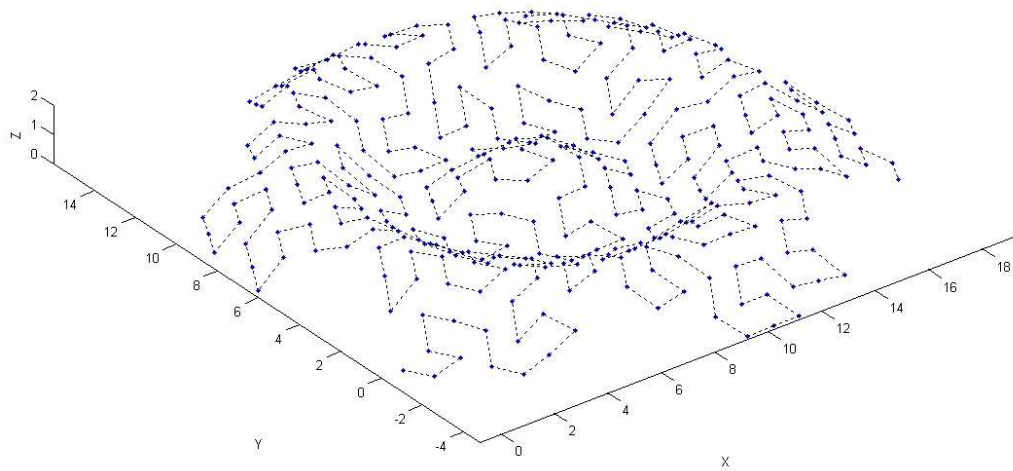


Figure 23 3-dimension view of conformed array.

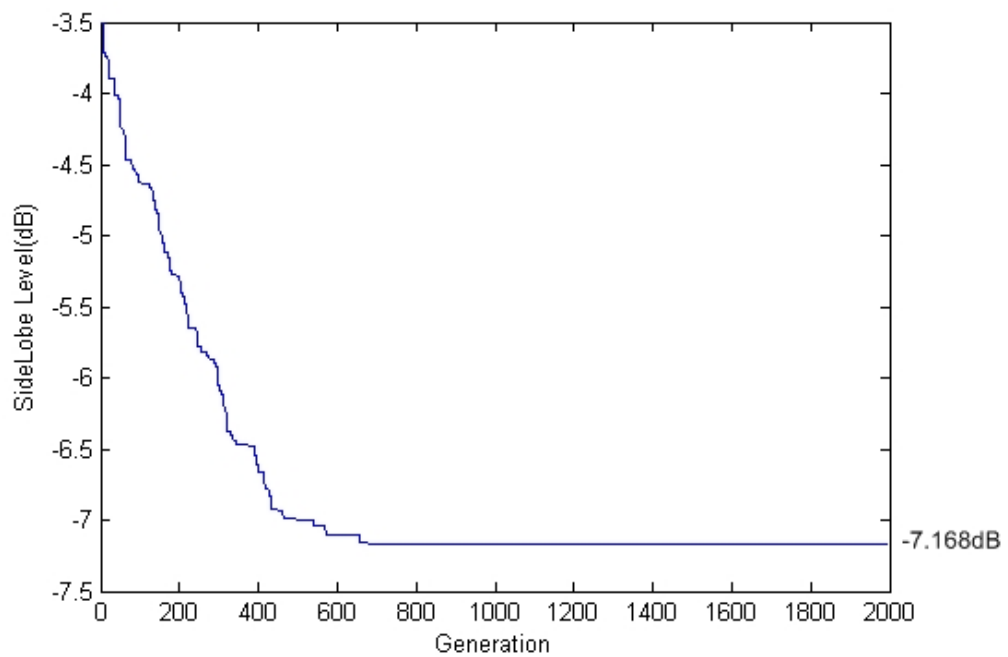
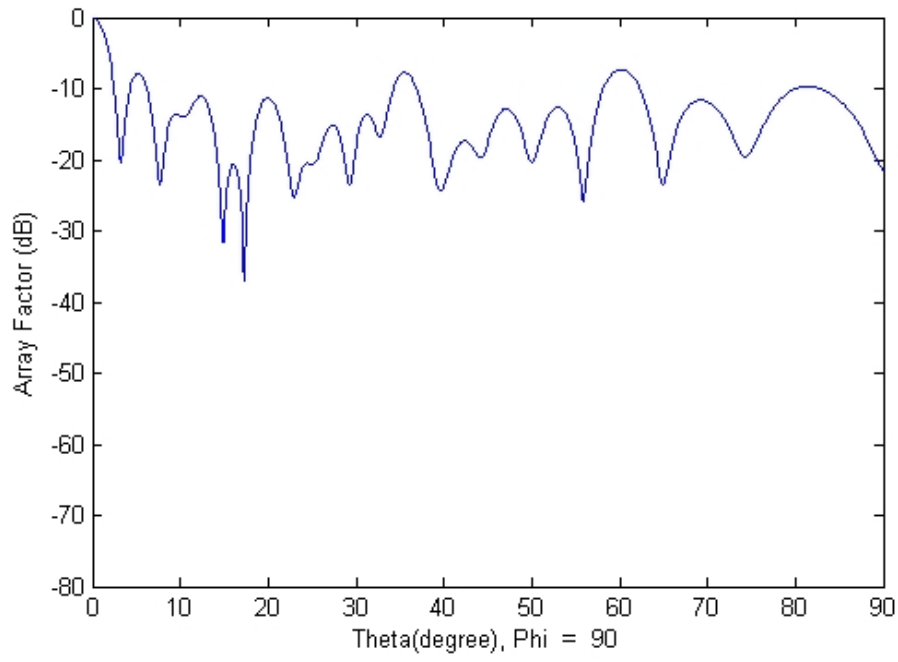
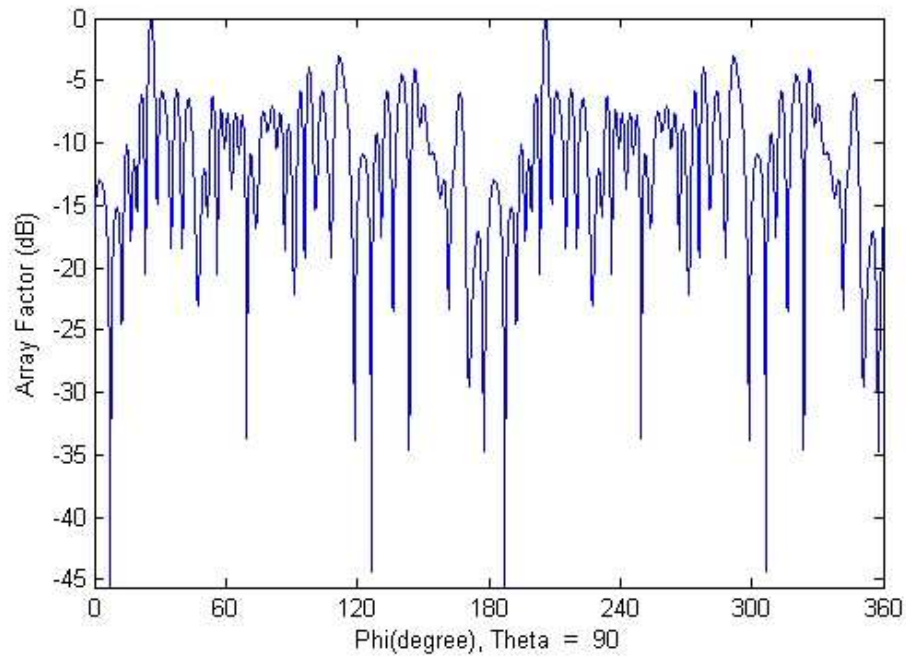


Figure 24 Evolution diagram of genetically optimized conformed array shows the reduction of sidelobe level from -3.5 dB to -7.168 dB.



(a)



(b)

Figure 25 Normalized genetically optimized array factor versus (a) θ for $\phi = 90^\circ$, (b) ϕ for $\theta = 90^\circ$, and (c) top view of the radiation pattern of the cosine-ring conformal array.

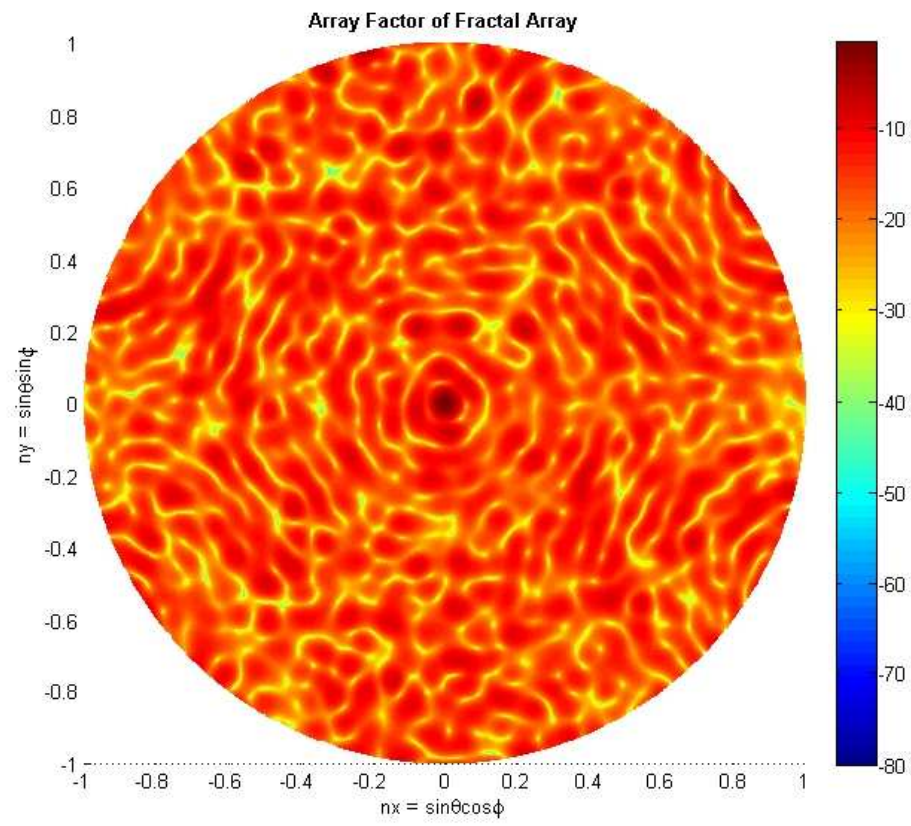


Figure 25 (continued)

2. Peano-gosper conformal arrays synthesis using genetic algorithm 2nd setting

We've reduced the current excitation on each element to binary and other settings remain the same. By this setting, we acquire the results of simulation as follow:

2.1 Simulation results of Peano-gosper array conformed to a cylindrical surface by x-axis

As the geometry is the same as 1.1 so we will not show that again. The results from GA are shown as follow:

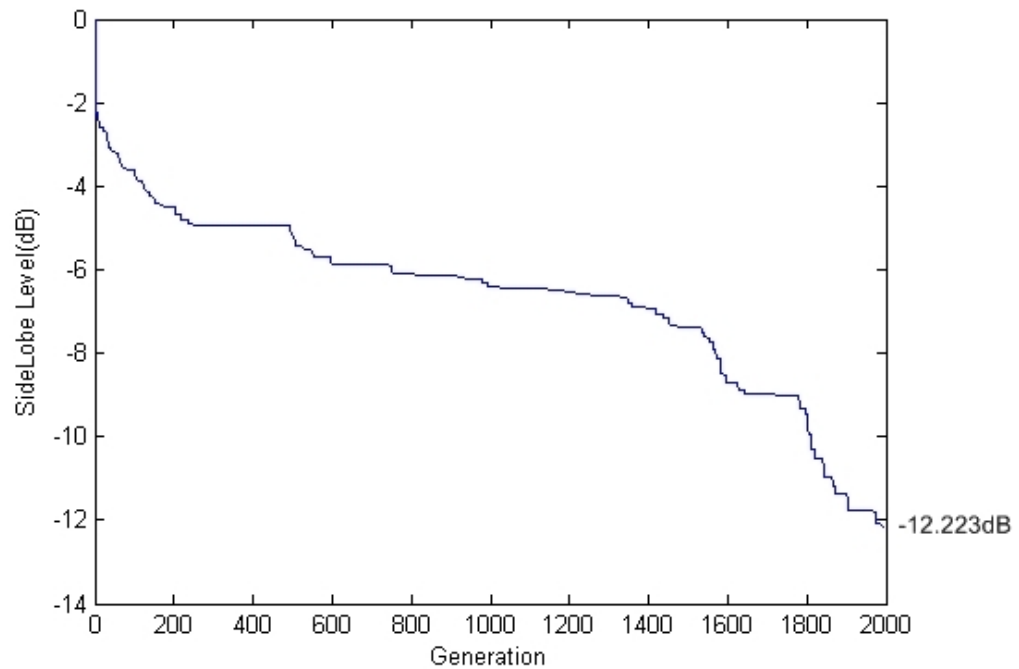
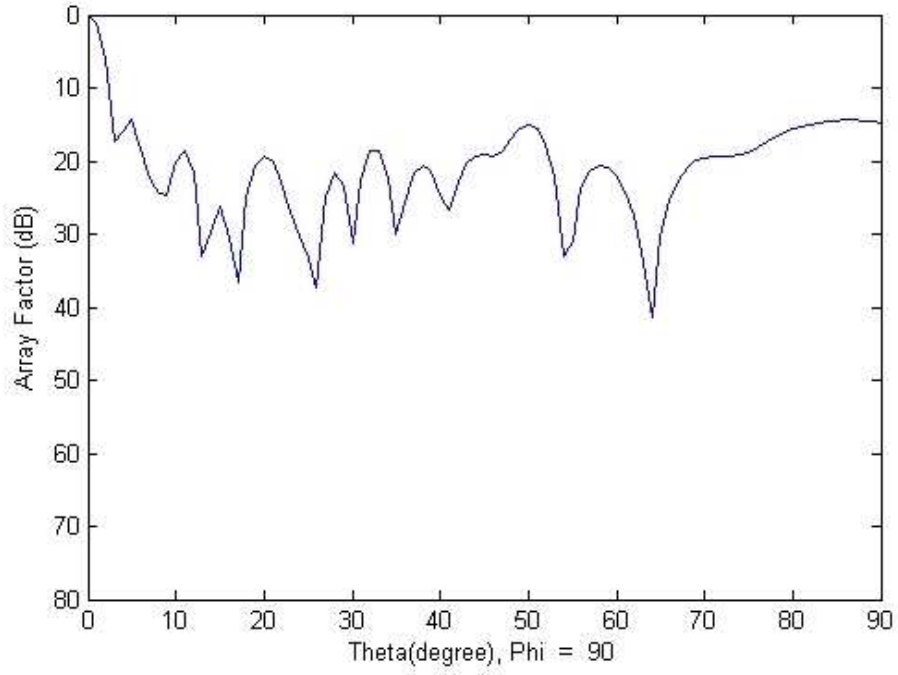
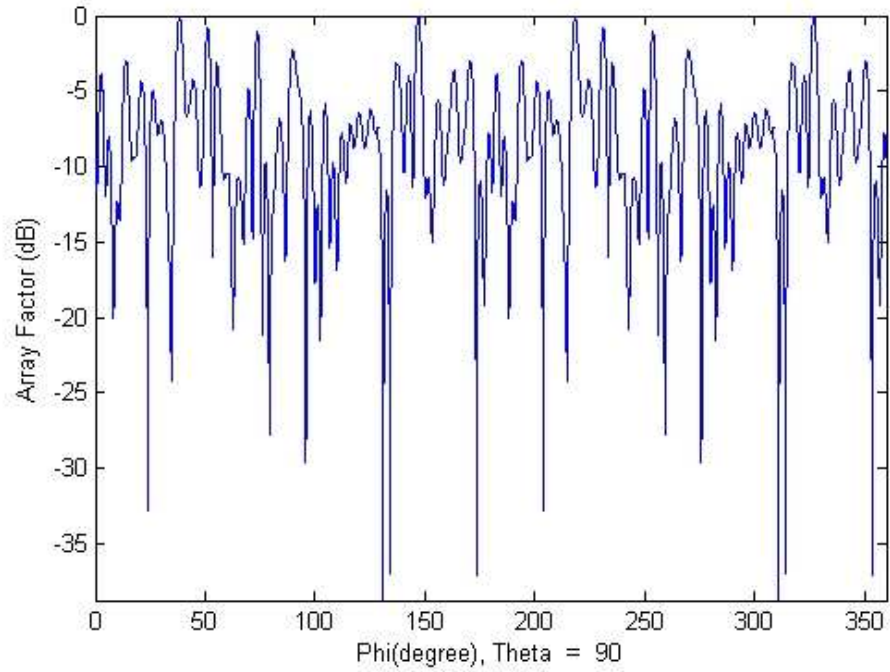


Figure 26 Evolution diagram of genetically optimized conformed array shows the reduction of sidelobe level from about -2 dB to -12.223 dB.



(a)



(b)

Figure 27 Normalized genetically optimized array factor versus (a) θ for $\phi = 90^\circ$, (b) ϕ for $\theta = 90^\circ$, and (c) top view of the radiation pattern of the x-axis cylindrical conformal array.

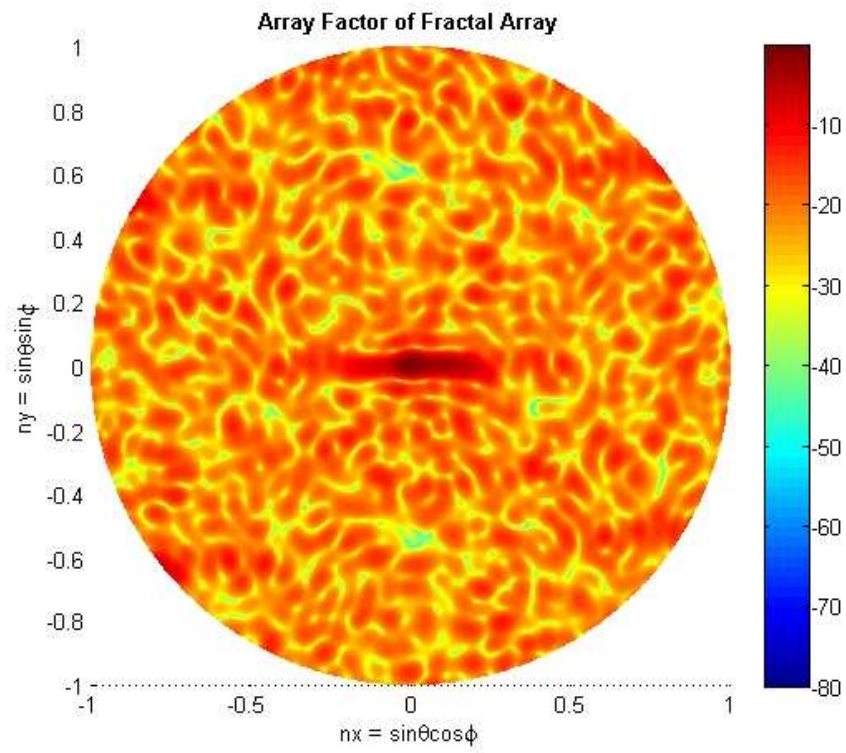


Figure 27 (continued)

2.2 Simulation results of Peano-gosper array conformed to a cylindrical surface by y-axis

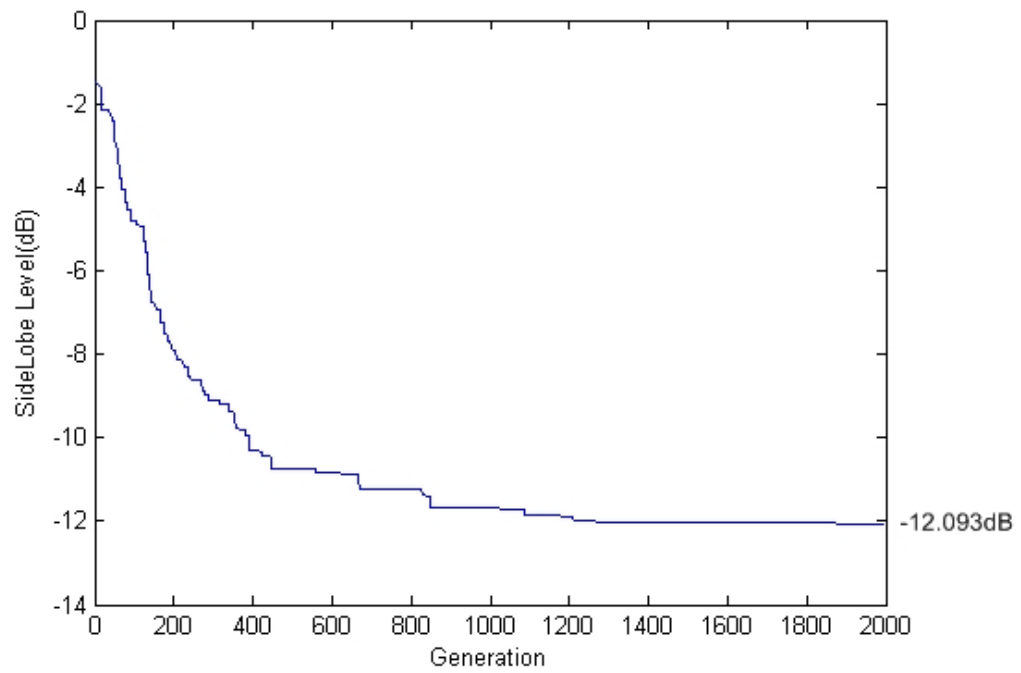
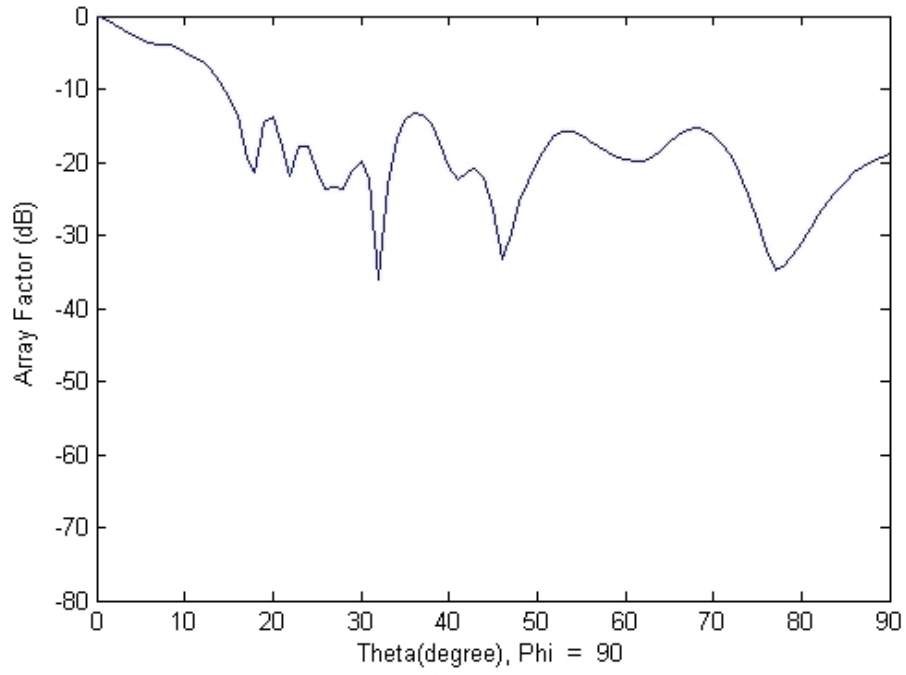
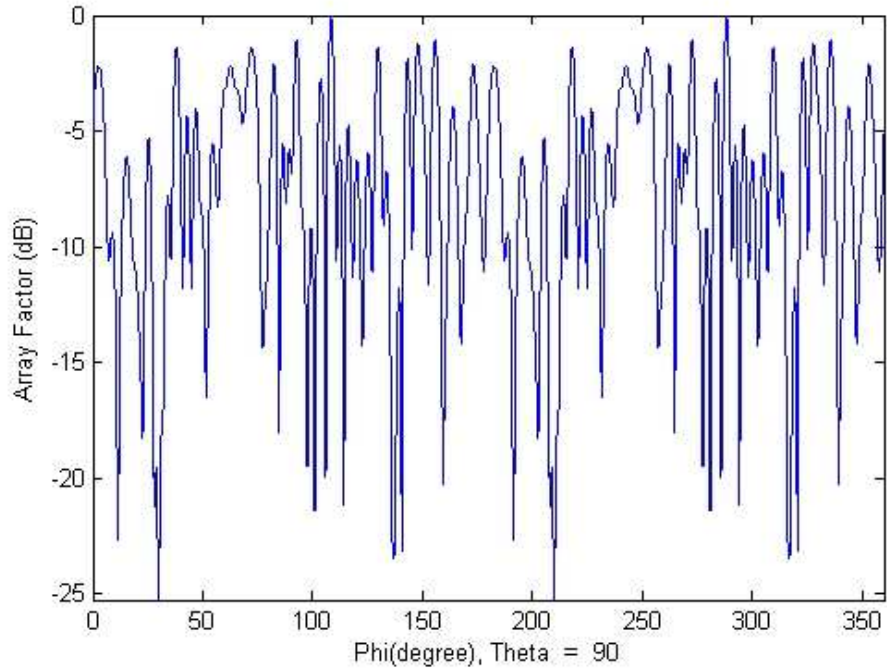


Figure 28 Evolution diagram of genetically optimized conformed array shows the reduction of sidelobe level from about -1 dB to -12.093 dB.

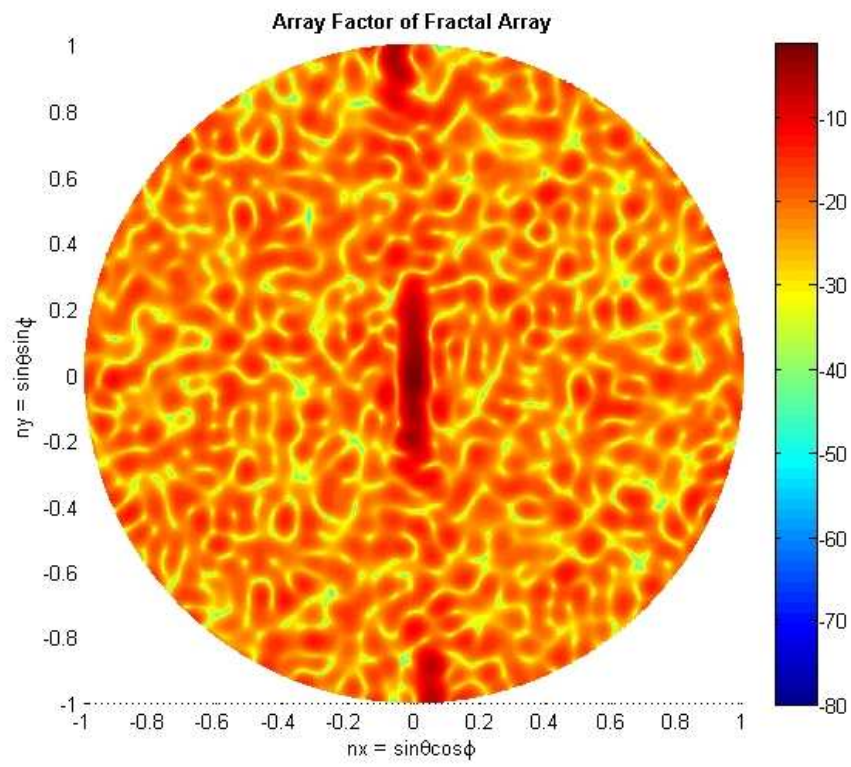


(a)



(b)

Figure 29 Normalized genetically optimized array factor versus (a) θ for $\varphi = 90^\circ$, (b) φ for $\theta = 90^\circ$, and (c) top view of the radiation pattern of the y-axis cylindrical conformal array.



(c)

Figure 29 (continued)

2.3 Simulation results of Peano-gosper array conformed to a cosine-ring surface

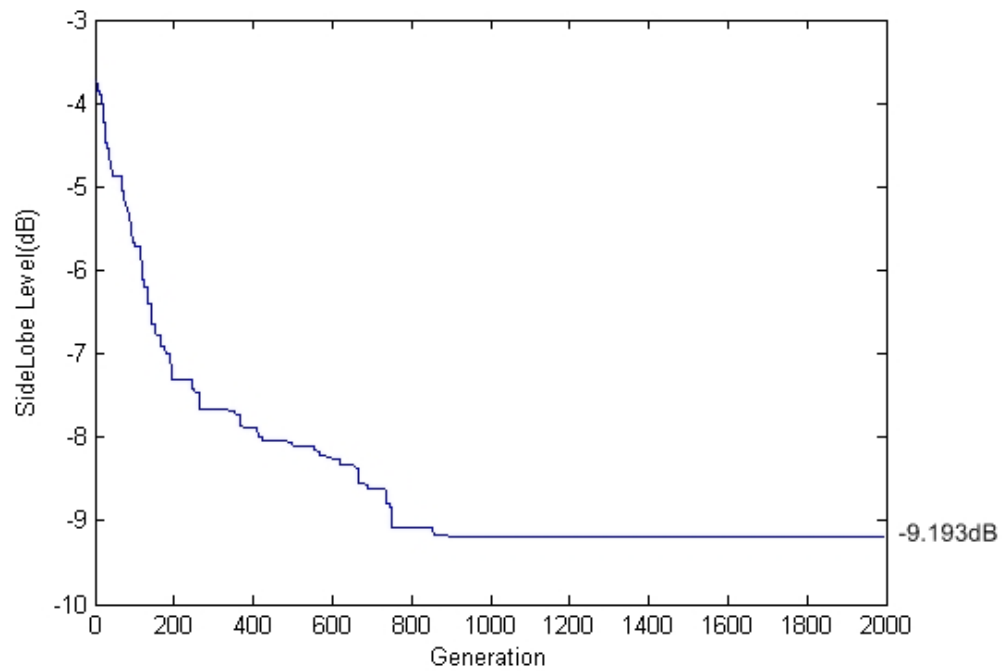
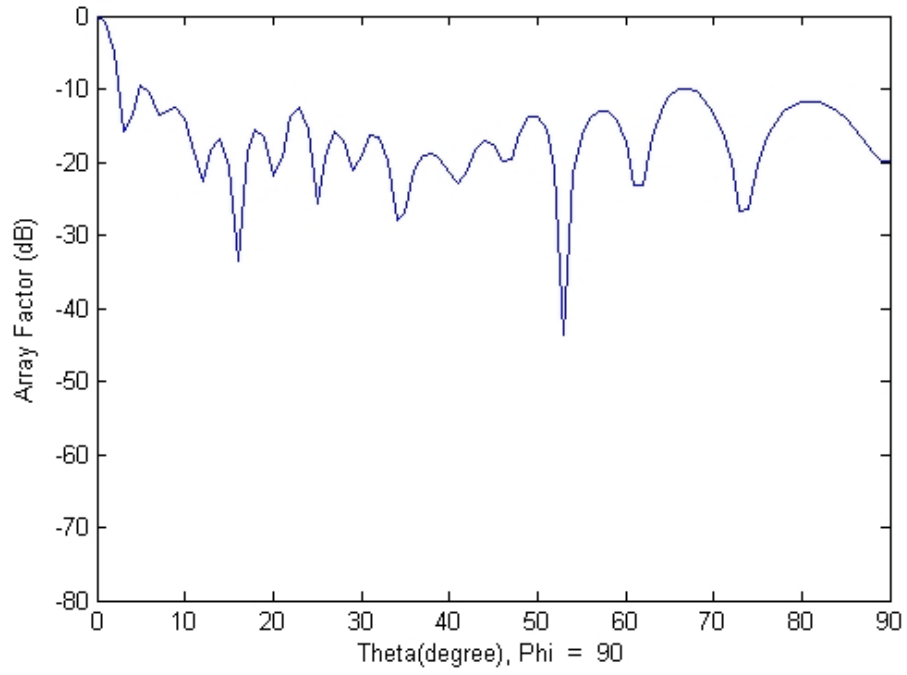
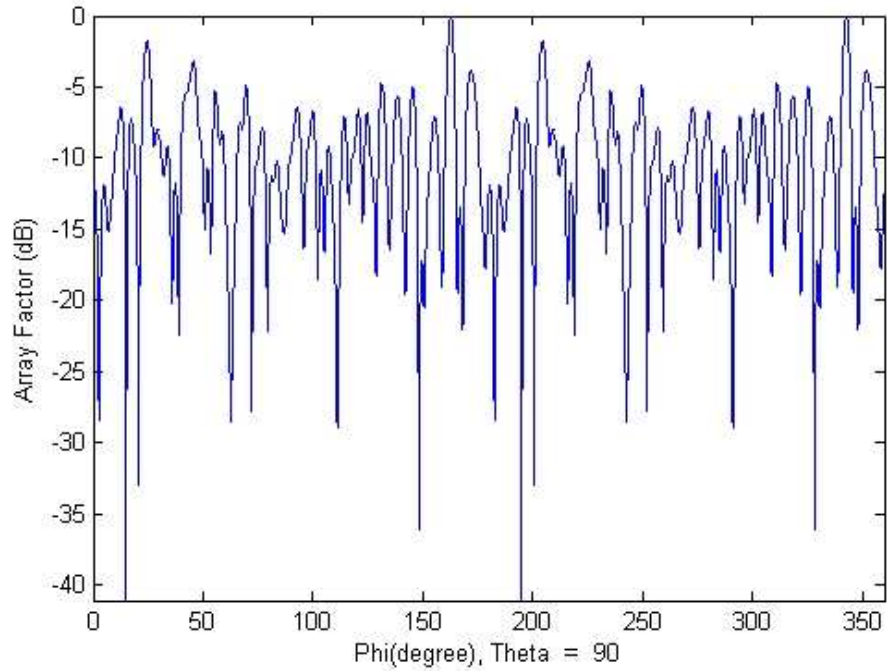


Figure 30 Evolution diagram of genetically optimized conformed array shows the reduction of sidelobe level from about -3.7 dB to -9.193 dB.

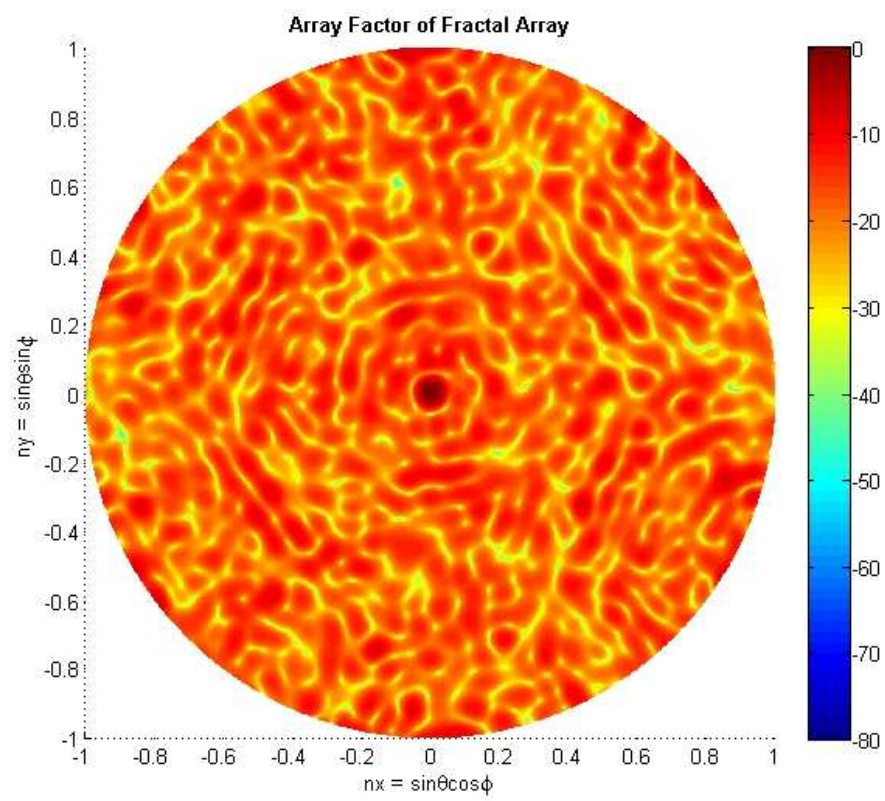


(a)



(b)

Figure 31 Normalized genetically optimized array factor versus (a) θ for $\phi = 90^\circ$, (b) ϕ for $\theta = 90^\circ$, and (c) top view of the radiation pattern of the cosine-ring conformal array.



(c)

Figure 31 (continued)

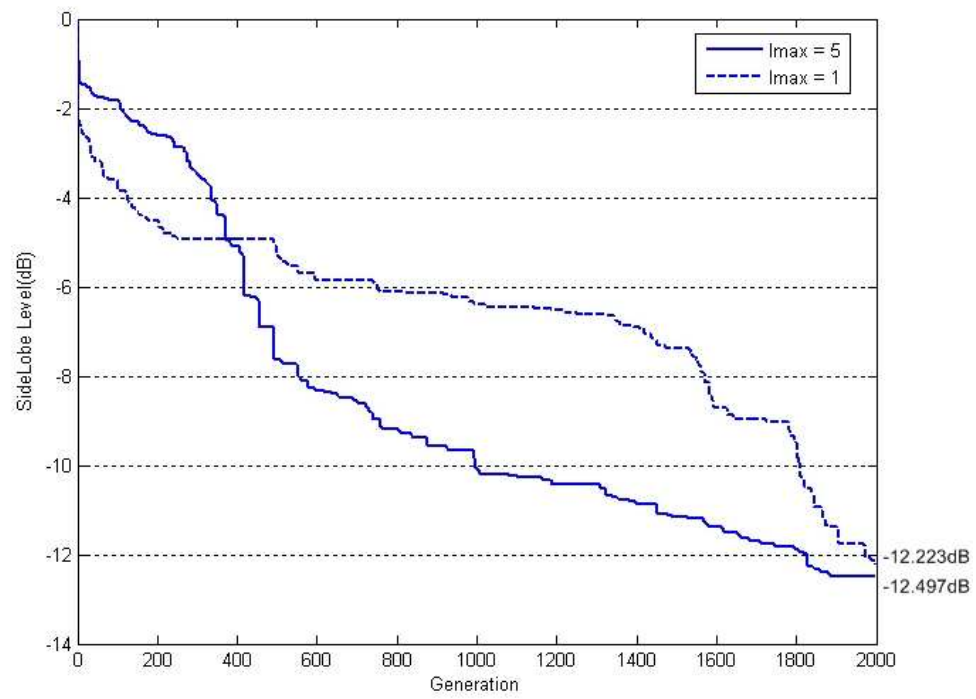
Discussion

After we've performed the simulation of the conformal Peano-gosper array by using genetic algorithm to optimize sidelobe level for all selected models with various setting parameters, we can draw out some picture from the solutions that acquired. First of all, the results show that our models contain unchanged Peano-gosper curve pattern on the top view as shown in Figure 14(c), 18(c) and 22(c).

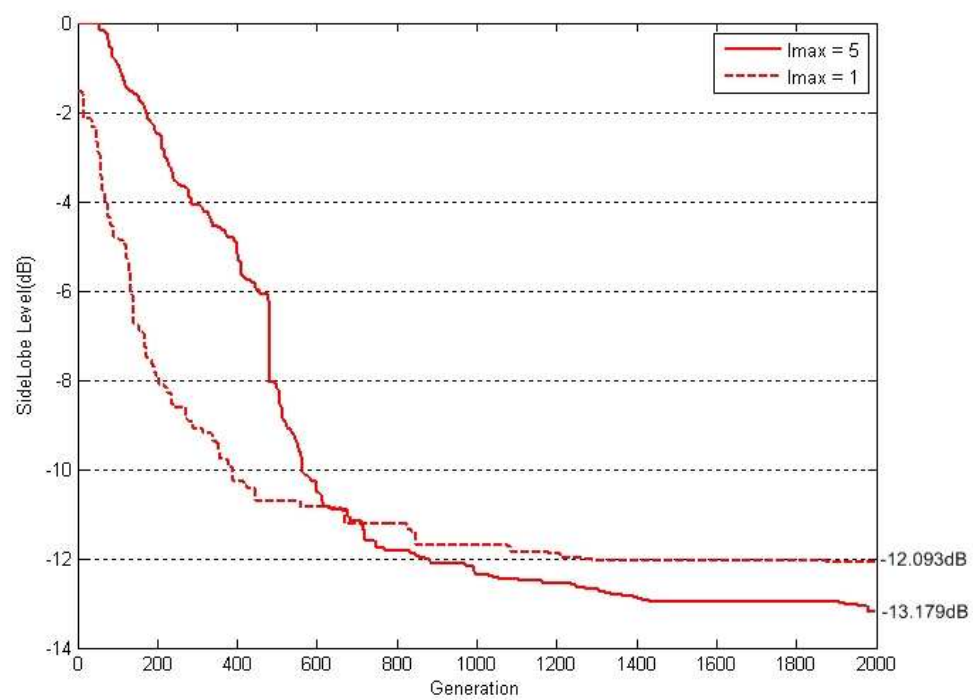
Second, with the concept of genetic algorithm we are capable of reducing the sidelobe level from high level to reasonable level for each model as shown in Figure 16, 20, 24, 26, 28 and 30. Therefore, consider each conformal surfaces that affect to the arrays, the results show that radiation pattern of each conformal arrays is depended on shape of the conformed surface also if we determine through Figure 17(c), 21(c) and 25(c) or Figure 27(c), 29(c) and 31(c).

We are now comparing the genetically optimized sidelobe level of the experimental arrays. Regarding to Figure 14 to 31, Figure 32 shows the comparison of sidelobe level between the model applying maximum current excitation at 5 and 1 ($I_{max} = 5$ vs. $I_{max} = 1$) via evolution diagrams, Figure 33 shows the comparison between each models and Table 5 show the summarized result of this thesis.

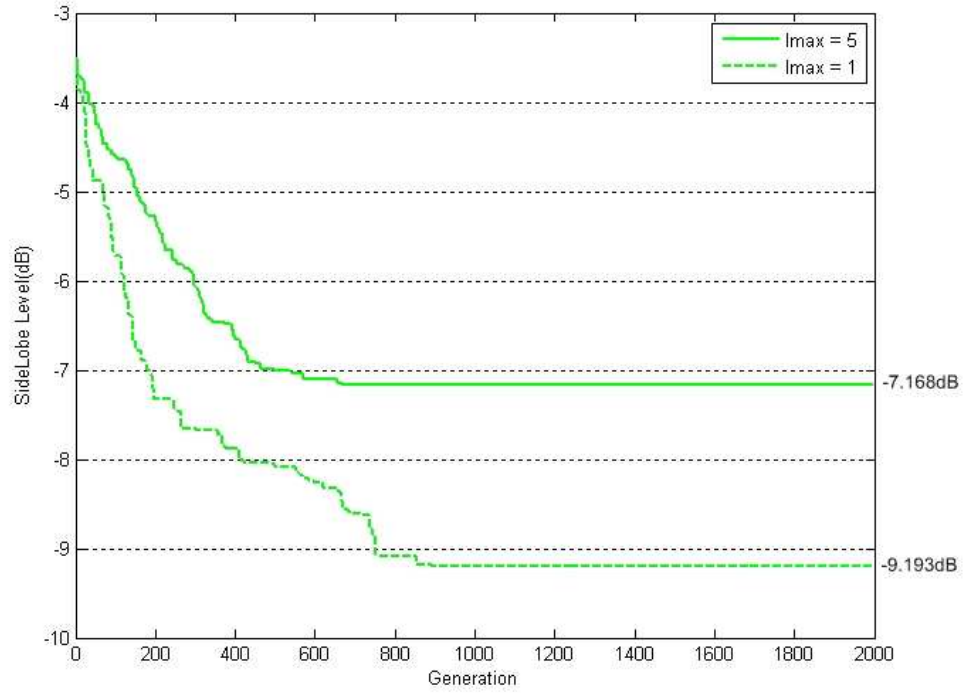
We analyze the other results of simulations which are 2000th iteration's arrangements of current excitation by testing each model's arrangement on different frequency by alternating element's minimum distance (d_{min}) to $\lambda/2$ and $3\lambda/4$. Figure 34 to 39 show the radiation pattern of each model in various d_{min} . As the figures have shown the frequency has some effect to the size and shape of radiation pattern but still remain the main pattern of its models.



(a)



(b)

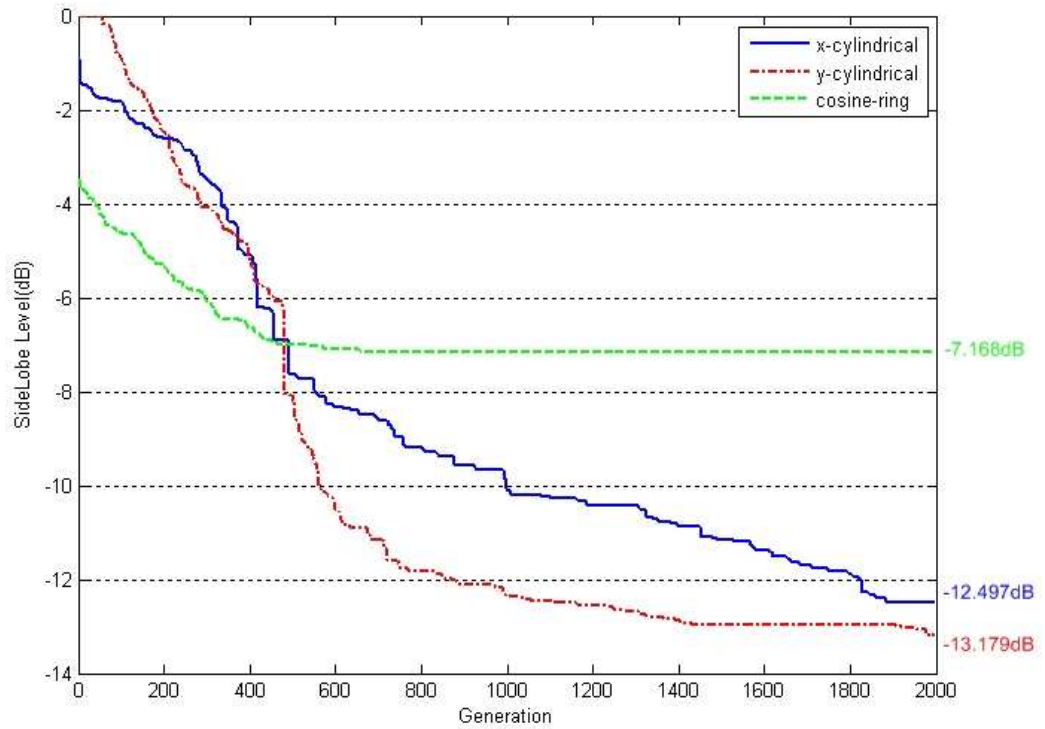


(c)

Figure 32 Evolution diagrams show the comparison of the sidelobe level for each models between current excitation maximum (I_{max}) equal to 5 (solid line) and 1 (dash line) (a) x-axis cylindrical conformal array, (b) y-axis cylindrical conformal array, and (c) cosine-ring surface conformal array.

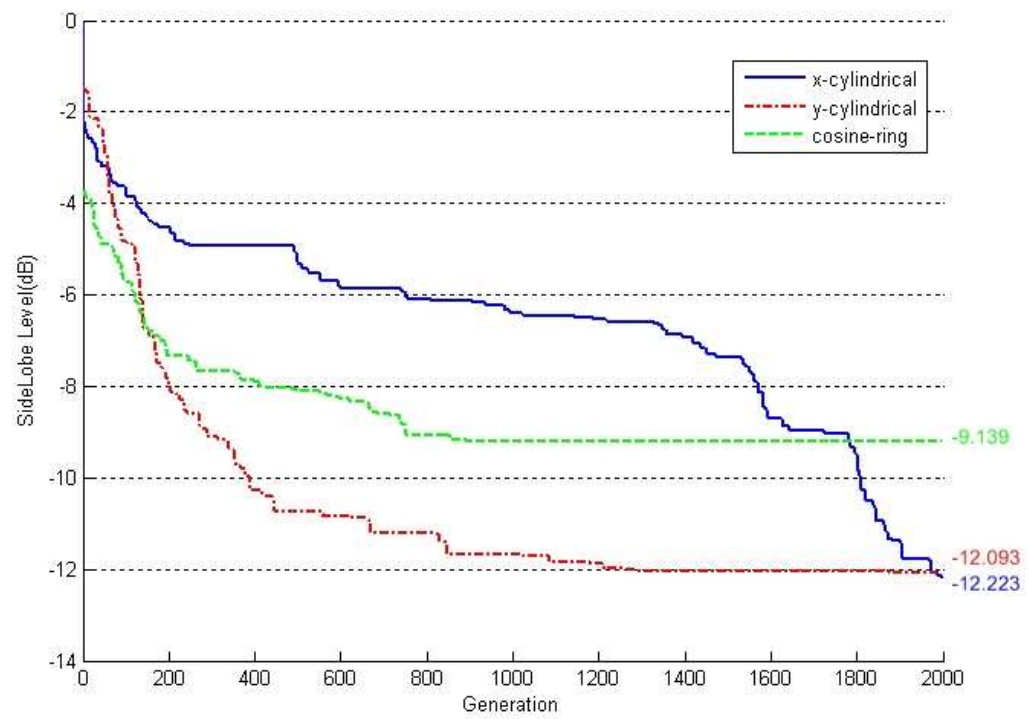
Table 5 Summarized results of the experiments

<i>Maximum current excitation</i>	<i>Conformed surface</i>	<i>Sidelobe level at 1st generation (dB)</i>	<i>Sidelobe level at 2000th generation (dB)</i>	<i>Reduced Sidelobe (dB)</i>
5	x-axis cylindrical	- 0.947 dB	- 12.497 dB	11.550
5	y-axis cylindrical	0 dB	- 13.179 dB	13.179
5	cosine-ring surface	- 3.284 dB	- 7.168 dB	3.884
1	x-axis cylindrical	0 dB	- 12.223 dB	12.223
1	y-axis cylindrical	- 0.651 dB	- 12.093 dB	11.442
1	cosine-ring surface	- 3.737 dB	- 9.139 dB	5.402



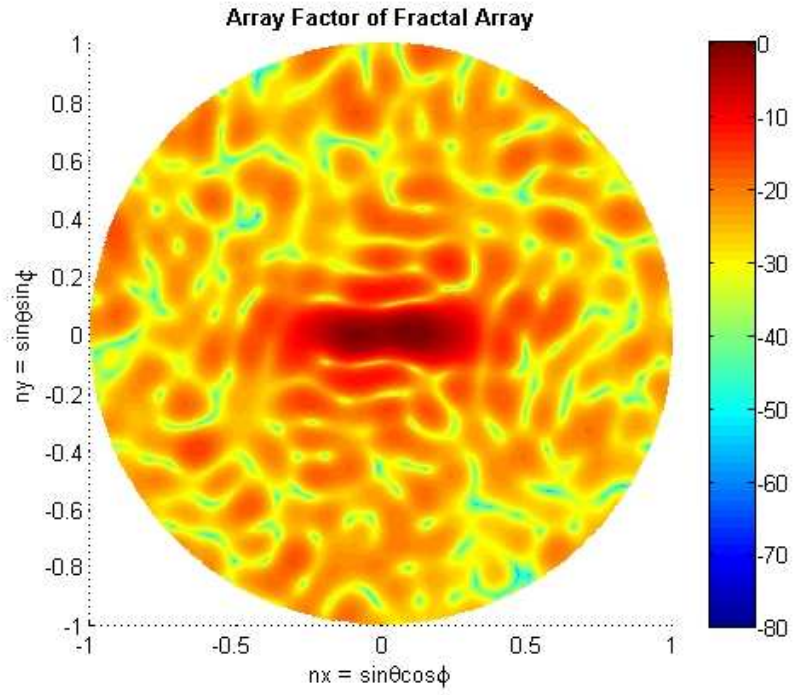
(a)

Figure 33 Evolution diagram shows comparison of sidelobe level between each models for (a) the maximum current excitation equal to 5 and (b) the maximum current excitation equal to 1, solid line as x-axis cylindrical, dash-dot line as y-axis cylindrical and dash line as cosine-ring.

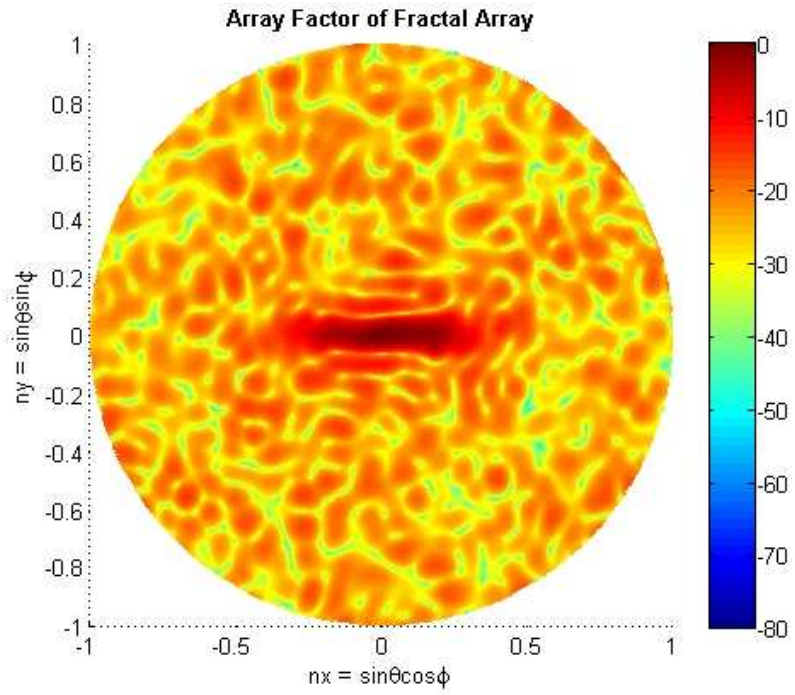


(b)

Figure 33 (continued)



(a)



(b)

Figure 34 Radiation pattern of 2000th generation x-cylindrical conformal array that the maximum current excitation equals to 5 at different sizes of minimum spacing (d_{min}): (a) $\lambda/2$, (b) $3\lambda/4$, and (c) λ .

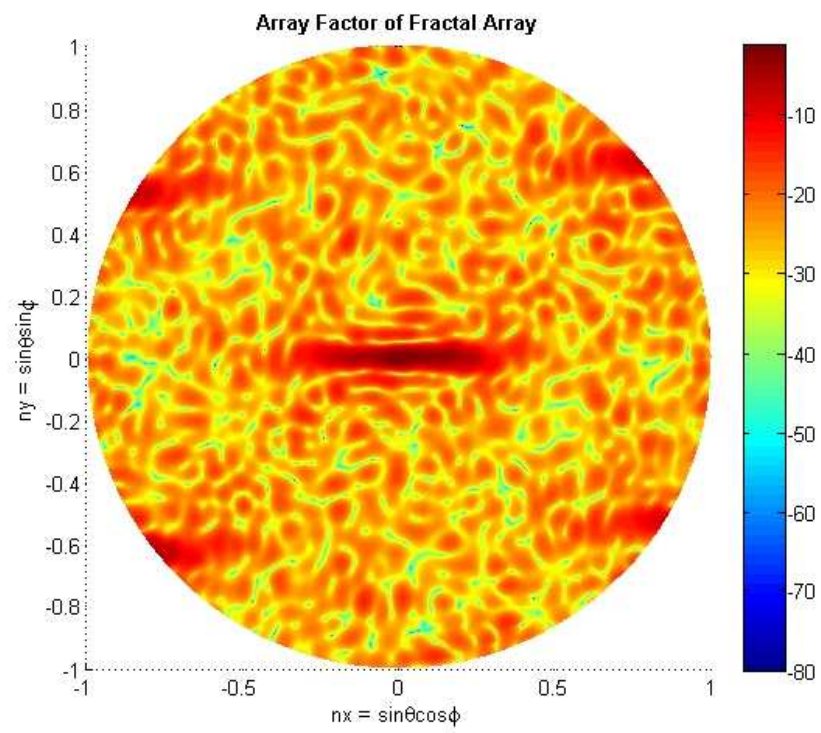
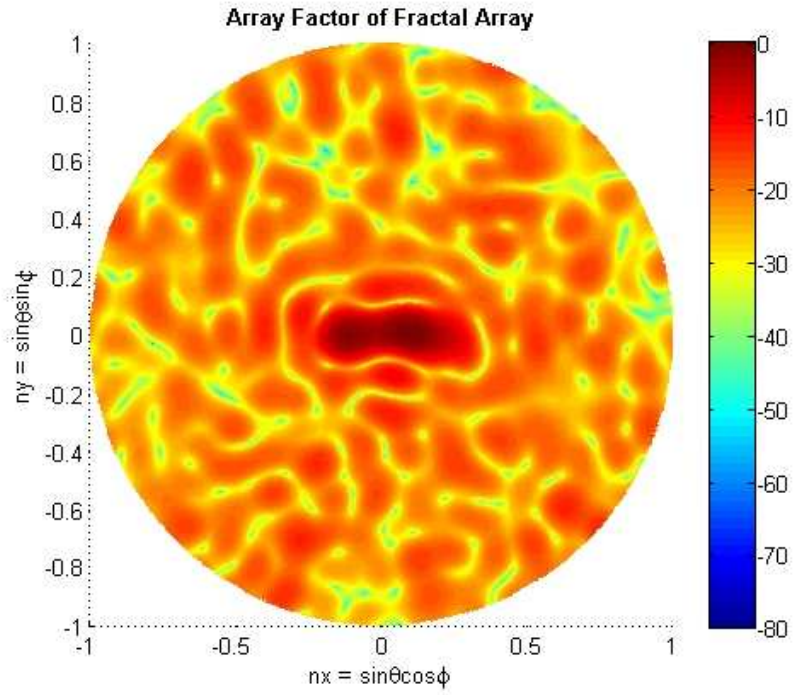
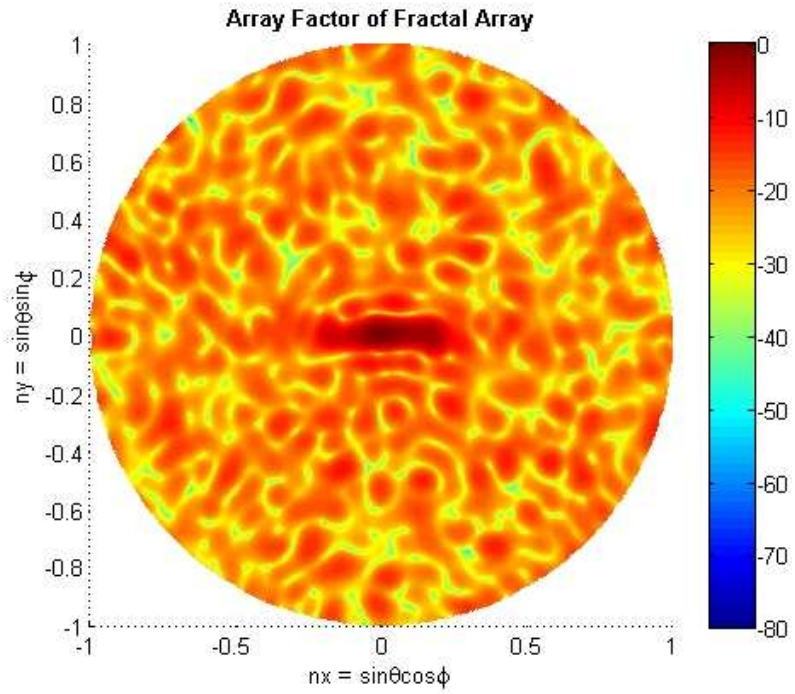


Figure 34 (continued)

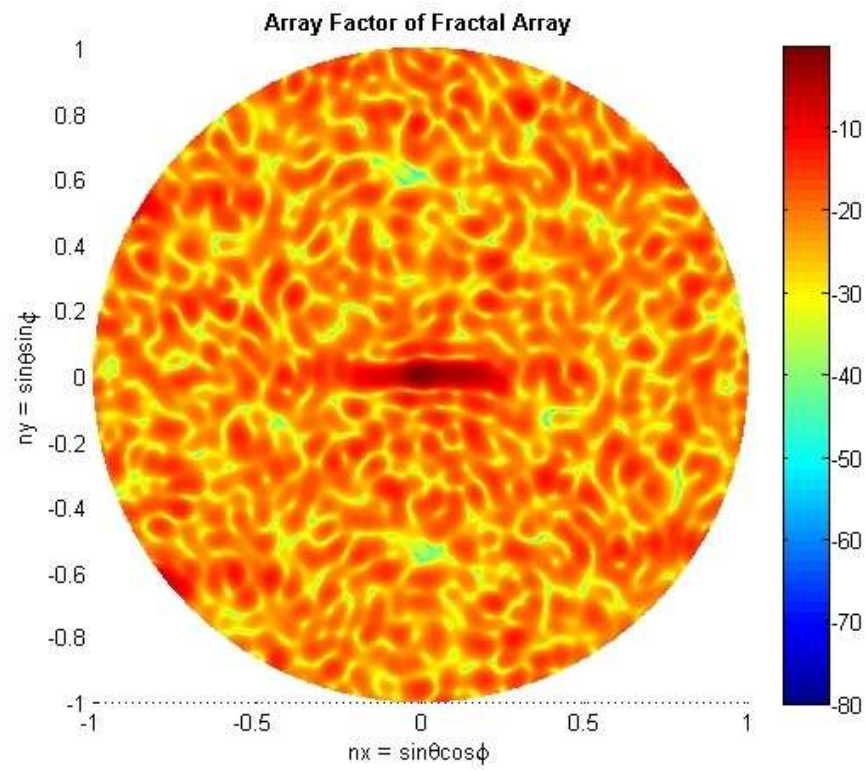


(a)



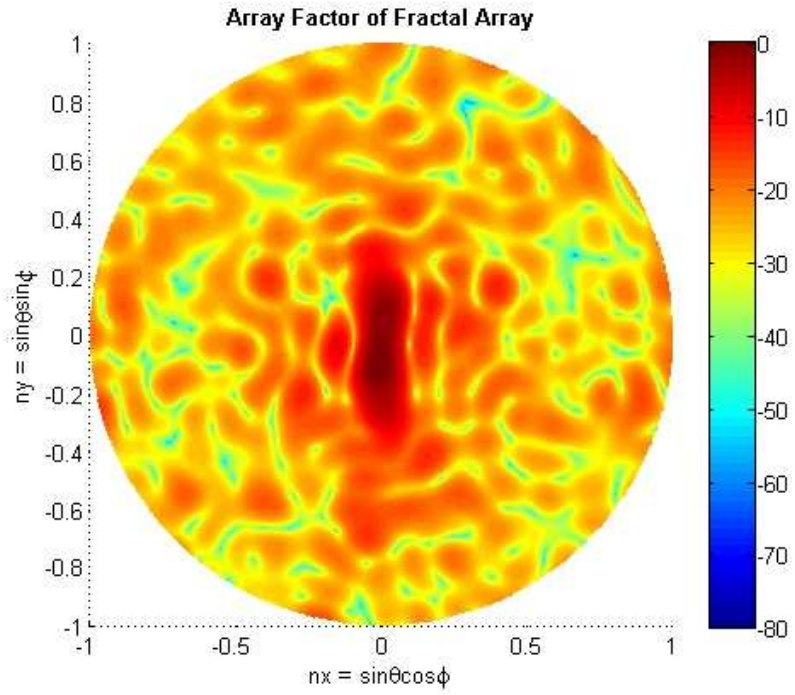
(b)

Figure 35 Radiation pattern of 2000th generation x-cylindrical conformal array that the maximum current excitation equals to 1 at different sizes of minimum spacing (d_{min}): (a) $\lambda/2$, (b) $3\lambda/4$, and (c) λ .

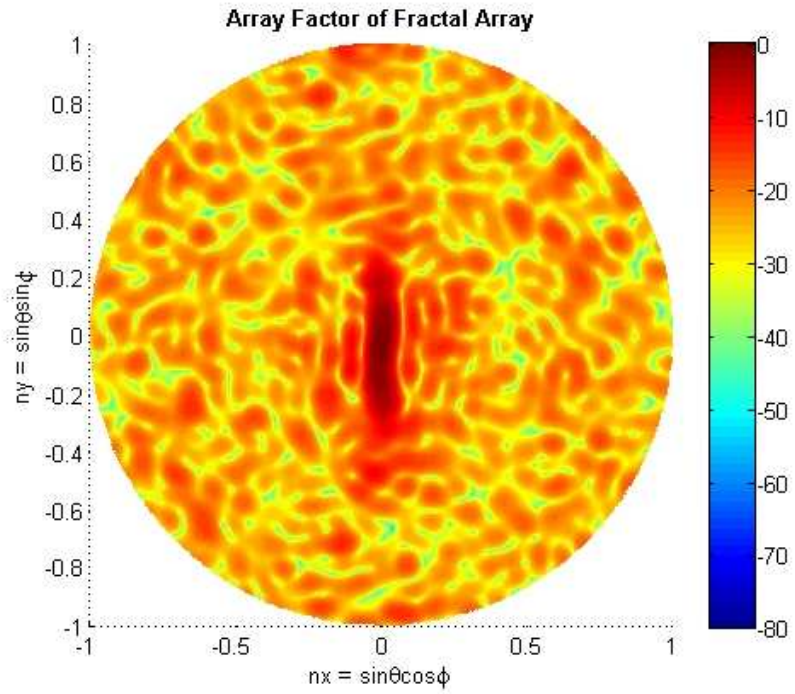


(c)

Figure 35 (continued)

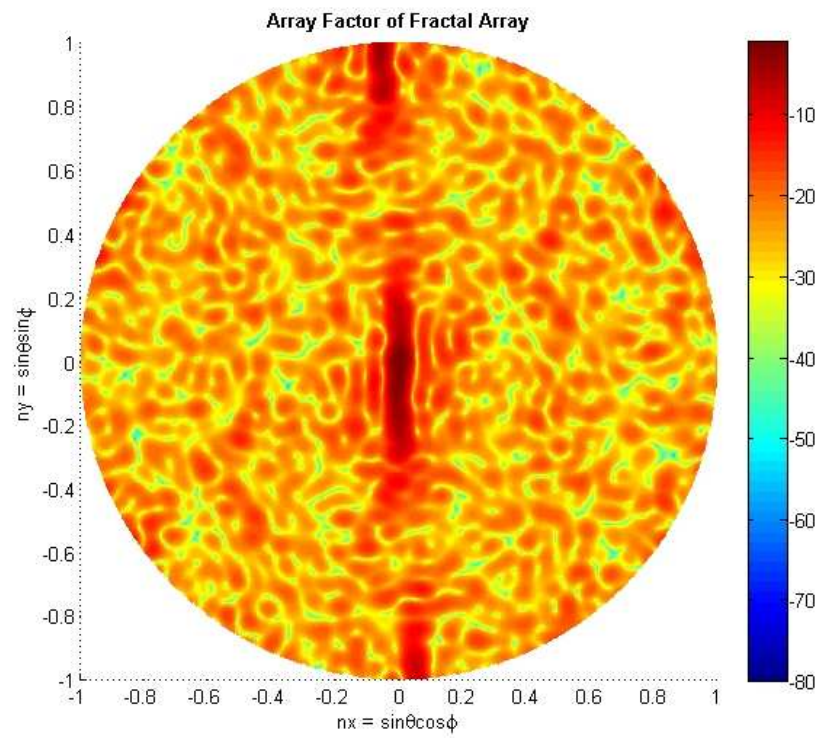


(a)



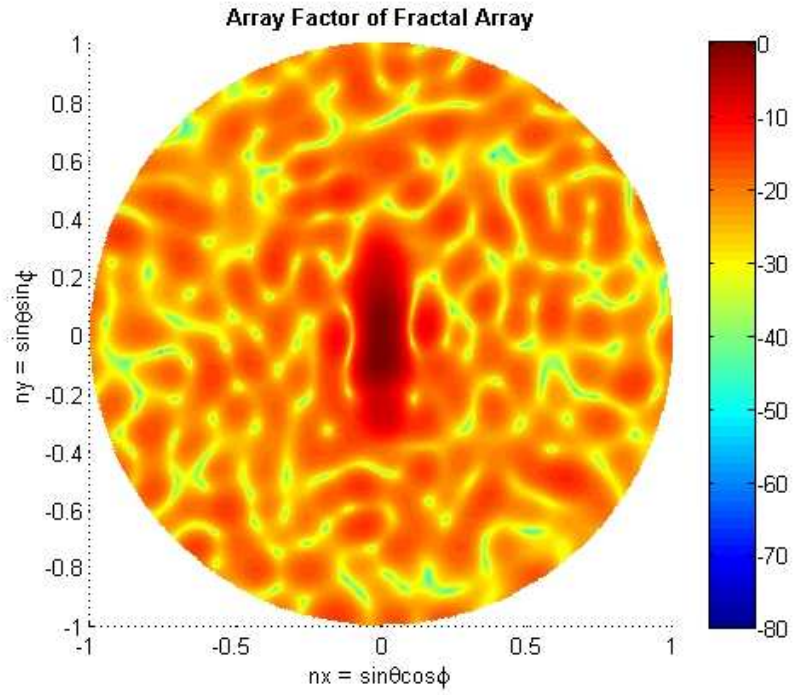
(b)

Figure 36 Radiation pattern of 2000th generation y-cylindrical conformal array that the maximum current excitation equals to 5 at different sizes of minimum spacing (d_{min}): (a) $\lambda/2$, (b) $3\lambda/4$, and (c) λ .

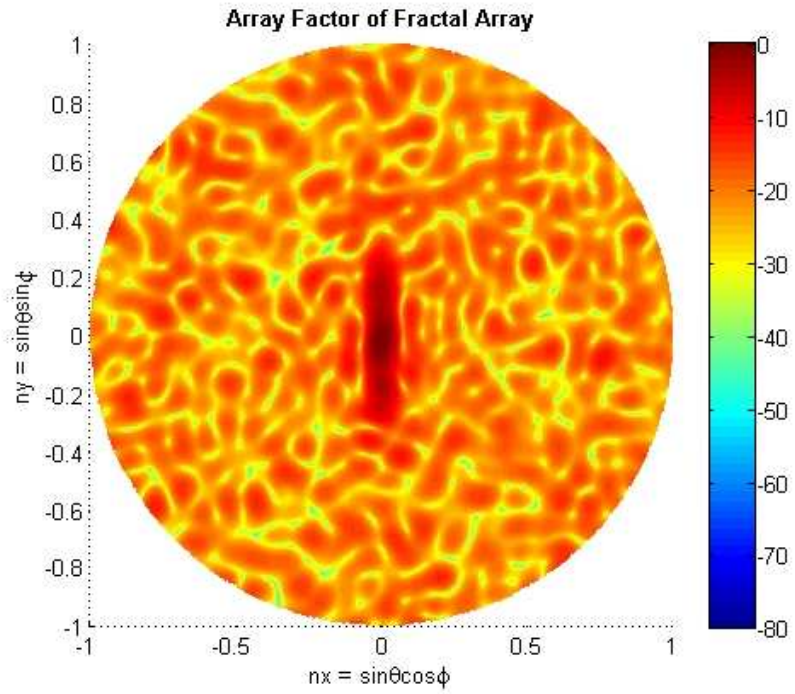


(c)

Figure 36 (continued)

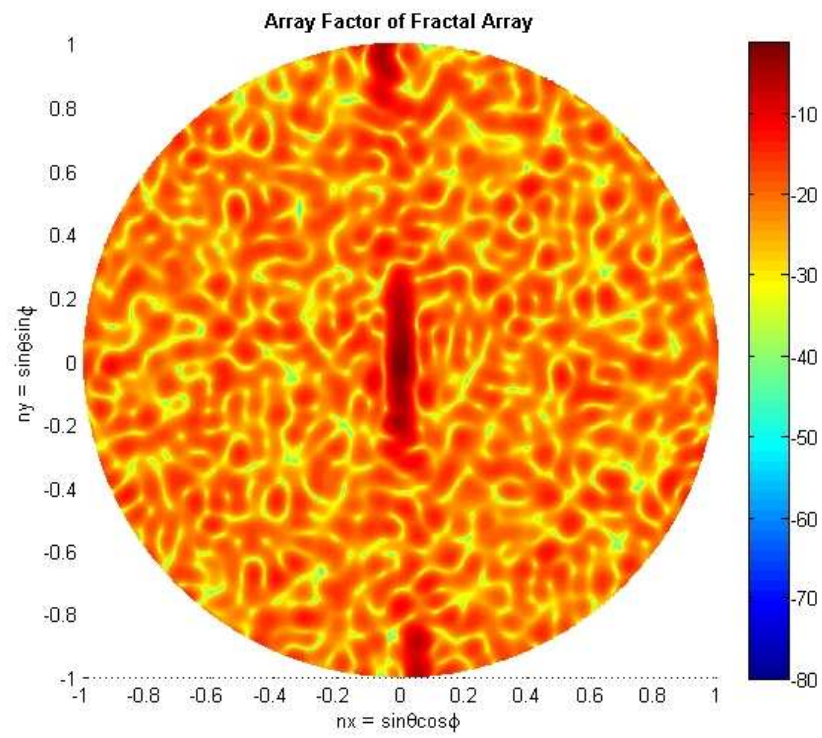


(a)



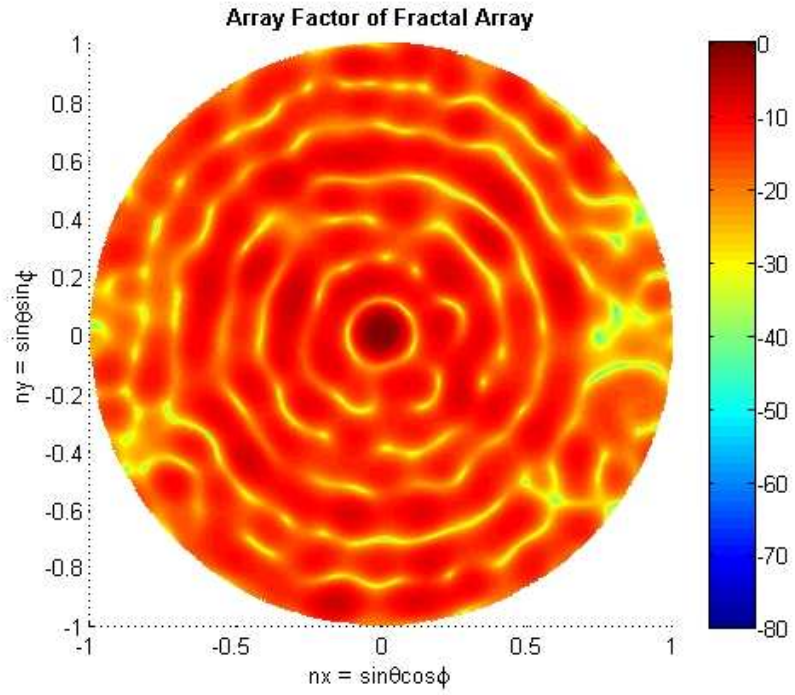
(b)

Figure 37 Radiation pattern of 2000th generation y-cylindrical conformal array that the maximum current excitation equals to 1 at different sizes of minimum spacing (d_{min}): (a) $\lambda/2$, (b) $3\lambda/4$, and (c) λ .

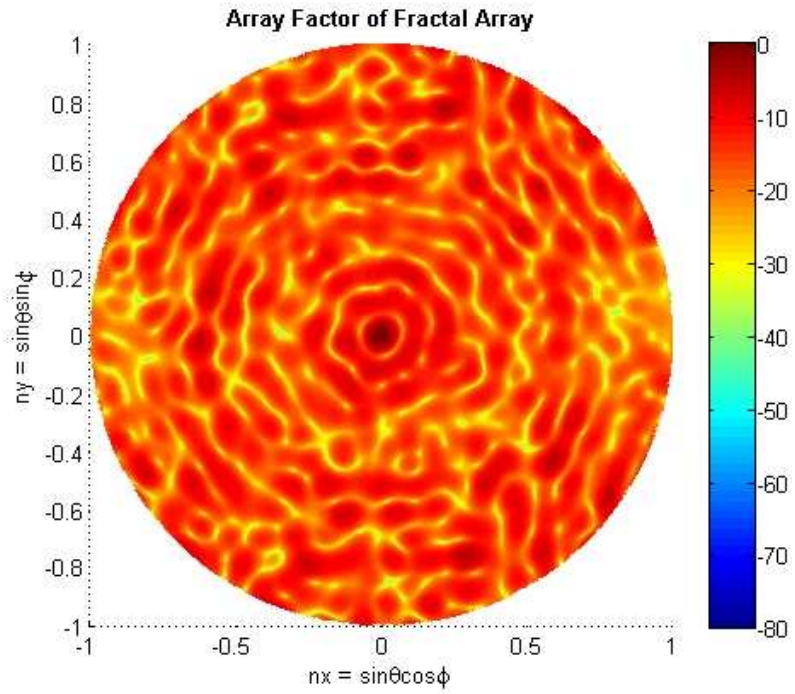


(c)

Figure 37 (continued)



(a)



(b)

Figure 38 Radiation pattern of 2000th generation cosine-ring conformal array that the maximum current excitation equals to 5 at different sizes of minimum spacing (d_{min}): (a) $\lambda/2$, (b) $3\lambda/4$, and (c) λ .

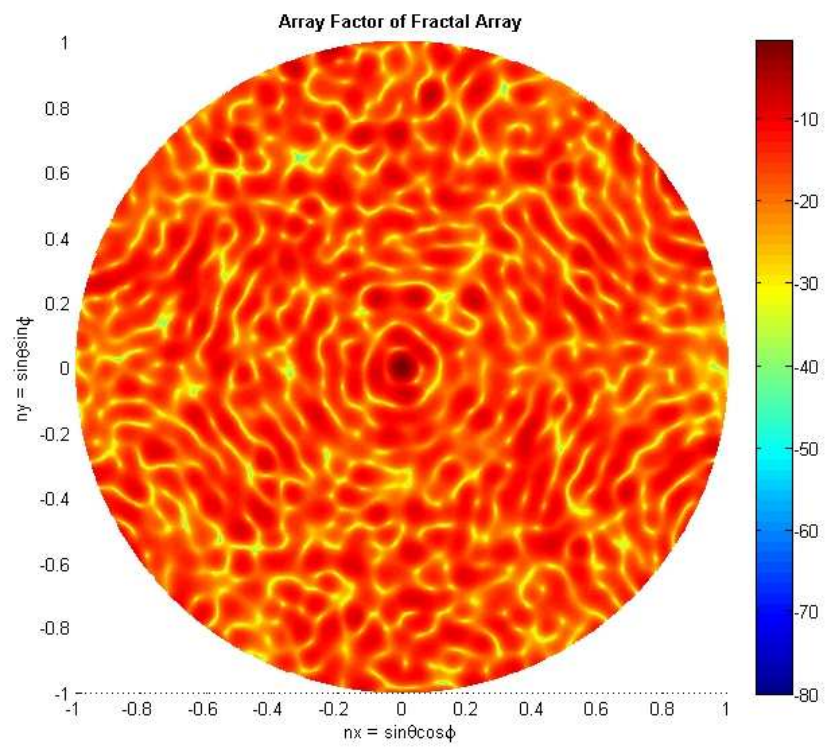
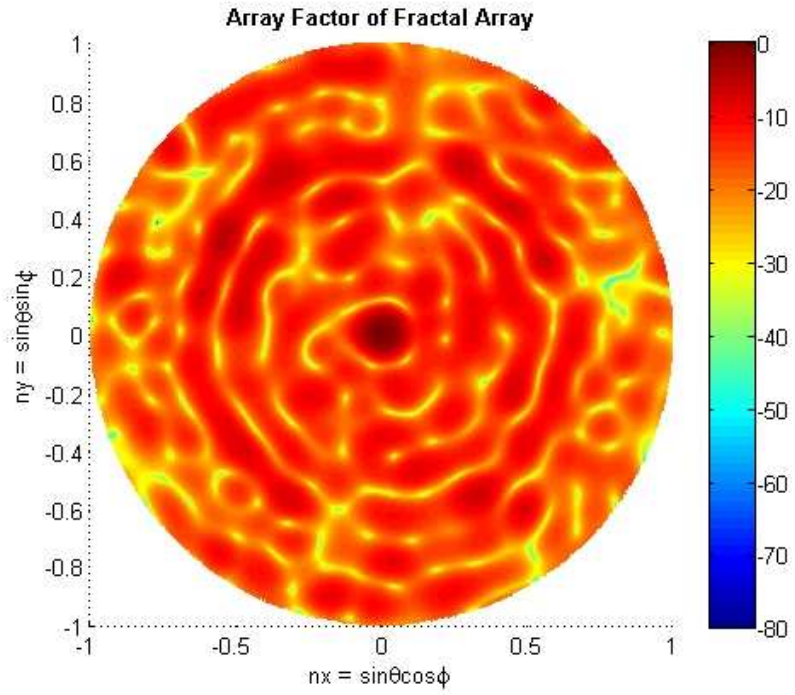
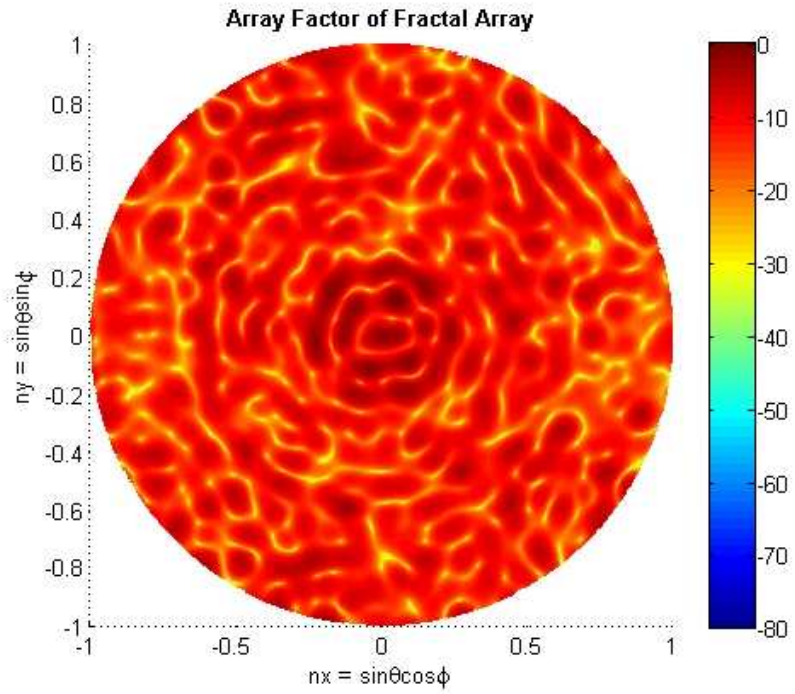


Figure 38 (continued)

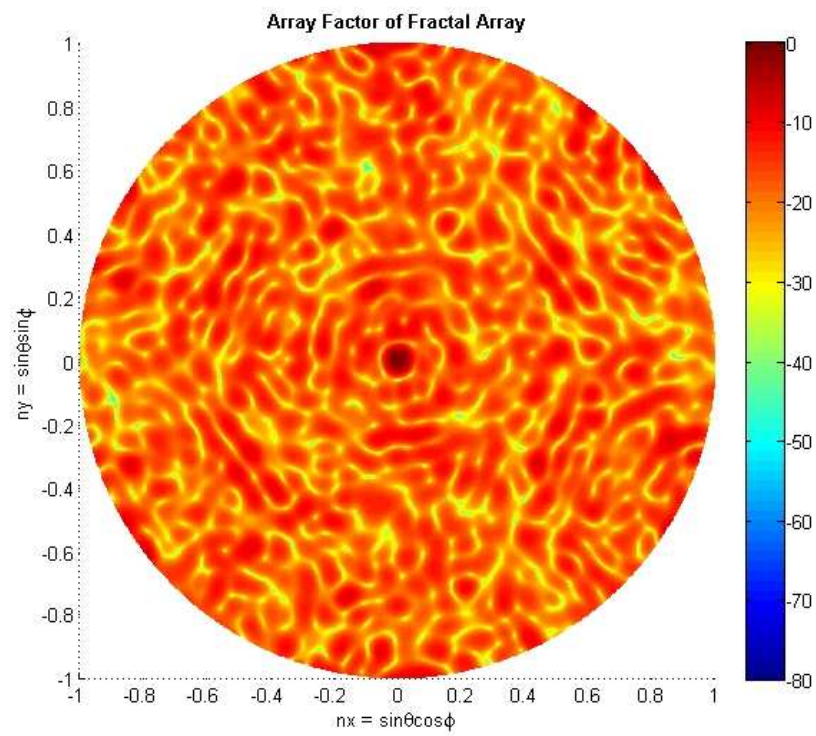


(a)



(b)

Figure 39 Radiation pattern of 2000th generation cosine-ring conformal array that the maximum current excitation equals to 1 at different sizes of minimum spacing (d_{min}): (a) $\lambda/2$, (b) $3\lambda/4$, and (c) λ .



(c)

Figure 39 (continued)

CONCLUSION AND RECOMMENDATION

Conclusion

The Peano-gosper based conformal arrays have been presented with sidelobe reduction on various surfaces, x-axis cylindrical, y-axis cylindrical and cosine-ring surface. It has been shown that the sidelobe level was reduced from high sidelobe levels to acceptable levels, about -12dB and -13dB for cylindrical models, by using genetic algorithm concept optimization that we run for 2000 iterations. It is found that the different shape and size of conform surfaces has a major effect on how sidelobe level of the array decreasing and also has a major role in constructing the radiation pattern.

Recommendation

For further work, we may emphasize on shapes of conformed surfaces to be more realistic and substitute each element with others than isotropic point source such as dipole or patch which make our models be more practical. Genetic algorithm optimization drawback, like other optimization techniques, is time-consuming so we should also focus on improving the speed of genetic algorithm.

This study limitation which is the implementation of the isotropic point sources as the array's elements is not practical and the direction vector of each element may not point to the same direction. We have to add more parameters into the equations or derive new equations for different situations. The limitation also applies to the radiation pattern, which we had represented in 2-dimension view instead of actual 3-dimension, that shapes of radiation pattern may goes uncertainty if we vary the frequency or d_{min} as show in Figure 34 to 39.

LITERATURE CITED

- Arakaki, D., D. H. Werner and R. Mittra. 2000. A Technique for Analyzing Radiation from Conformal Antennas Mounted on Arbitrarily-Shaped Conducting Body, pp. 10-13. **Antennas and Propagation Society International Symposium, 2000.** IEEE.
- Balanis, C. 2005. **Antenna Theory: Analysis and Design.** John Wiley and Sons, Inc., New York.
- Bogard, J.N., D.H. Werner and P. L. Werner. 2004. A Comparison of the Peano-Gosper Fractile Array with the Regular Hexagonal Array. **Microwave and Optical Technology Letters**, 43(6): 524-526.
- Bondarenko, A.N. and Y.V. Mikhailova. 2005. Radiation Pattern Synthesis for Arrays Based on Sierpinski Gasket, pp. 39-42. **KORUS'2005.** IEEE.
- Bray, M. G., D. H. Werner, D. W. Boeringer and D. W. Machuga. 2002. Optimization of Thinned Aperiodic Linear Phased Arrays Using Genetic Algorithms to Reduce Grating Lobes During Scanning. **IEEE Transactions on Antennas and Propagation**, 50(11): 2919-2924.
- Falconer K. 2003. **Fractal Geometry Mathematical Foundations and Applications.** 2nd Edition. John Wiley and Sons, Inc., New York.
- Hansen, R.C. 2003. **Phased Array Antennas.** John Wiley and Sons, Inc., New York.
- Haupt R. L. 1995. An Introduction to Genetic Algorithms for Electromagnetics. **IEEE Antennas and Propagation Magazine.** 37: 7-15.
- _____ and S. E. Haupt. 2003. **Practical Genetic Algorithms.** John Wiley and Sons, Inc., New York.

- Holder, E. J. 1991. Sidelobe Performance in Quadratic Phase Conformal Arrays. **IEEE Transactions on Antennas and Propagation**. 39: 1234-1237.
- Johnson, J. M. and Y. Rahmut-Samii. 1997. Genetic Algorithms in Engineering Electromagnetics. **IEEE Antennas and Propagation Magazine**. 39: 7-15.
- Josefsson, L. and P. Persson. 1999. Conformal Array Synthesis including Mutual Coupling. **Electronics Letters**. 35: 625-627.
- _____, _____. 2006. **Conformal Array Antenna Theory and Design**. John Wiley and Sons, Inc., New Jersey.
- Kraus, J. D. and R.J. Marhefka. 2003. **Antennas for All Applications**. McGraw-Hill, Singapore.
- Kim Y. and D. L. Jaggard. 1986. The Fractal Random Array, pp. 1278-1280. **Proceeding of the IEEE**. IEEE.
- Kuhirun W., 2003. **A New Design Methodology for Modular Broadband Arrays Based on Fractal Tilings**. Ph.D. Thesis, the Pennsylvania State University at University Park USA.
- _____, T. Jariyanorawiss, M. Polpasee, and N. Homsup. 2004. Solving for Current Distribution Using Gauss-Seidel Iteration and Multigrid Method. **Proceedings of the International Conference in ECTI**, Thailand.
- Mandelbrot, B. B. 1983. **The Fractal Geometry of Nature**. John Wiley and Sons, Inc., New York.

- Massa, A., M. Donelli, F. G.B. De Nataale, S. Caorsi and A. Lommi. 2004. Planar Antenna Array Control With Genetic Algorithms and Adaptive Array Theory. **IEEE Transactions on Antennas and Propagation**, 52: 2919-2924.
- Petko, J.S. and D.H. Wener. 2005. The Evolution of Optimal Linear Polyfractal Arrays Using Genetic Algorithms. **IEEE Transactions on Antennas and Propagation**, 53: 3604-3615.
- Polpasee, M. 2007. **Sidelobe Reduction in Peano-gosper Fractal Arrays Using Genetic Algorithms**. M.Eng. Thesis, Kasetsart University, Thailand.
- _____, and N. Homsup. 2006a. Peano-Gosper Fractal Array Synthesis Using Genetic Algorithms. **Ocean 2006 IEEE Asia Pacific**. Singapore.
- _____, _____. 2006b. Optimized low sidelobe level of Peano-Gosper Fractal Arrays Synthesis Using Genetic Algorithms. **Proceedings of the International Conference in ECTI**, Thailand.
- _____, _____. 2006c. Optimize Directivity Pattern for Arrays by Using Genetic Algorithms Based on Planar Fractal Arrays. **Proceedings of the International Conference in ISCIT**, Thailand.
- _____, _____ and W. Kuhirun. 2005. Analysis of Fractal Arrays Generated using a 3x3 Subarray Generator. **Proceedings of the International Conference in ECTI**, Thailand.
- Polpasee, M., W. Kuhirun and N. Homsup. 2005. Analysis of Fractal Arrays Generated using a 3x3 Subarray Generator, pp. 1485-1488. **Proceedings of the International Conference in ISCIT**, China.
- Schuman, H.K. 1994. Conformal Array Synthesis. **Antennas and Propagation Society International Symposium**, 1: 526-529

- Soltankarimi, F., J. Nourinia and Ch. Ghobadi. 2004. Sidelobe Level Optimization in Phased Array Antennas Using Genetic Algorithm, pp. 389-394. **ISSSTA 2004**, Australia.
- Thor, B. and L. Josefsson. 2003. Radiation and Scattering Tradeoff Design for Conformal Arrays. **IEEE Transaction on Antennas and Propagation**, 51: 1069-1076
- Villegas, F.J., T. Cwik, Y. Rahmat-Samii and M. Manteghi. 2004. A Parallel Electromagnetic Genetic-Algorithm Optimization (EGO) Application for Patch Antenna Design. **IEEE Transactions on Antennas and Propagation**, 52: 2424-2435.
- Vinoy, K.J. 2002. **Fractal Shaped Antenna Elements for Wide-and-Multi Band Wireless Application**. Ph.D. Thesis, The Pennsylvania State University at University Park USA.
- Virunha, P., M. Polpasee and N. Homsup. 2006. Optimized Directivity of Square-Planar Fractal Arrays Using Genetic Algorithms, pp. 28-31. **Ocean 2006 IEEE Asia Pacific**, Singapore.
- Wener, D. H. and P. L. Werner. 1999. A General Class of Self-Scalable and Self-Similar Arrays, pp. 2882-2885. **Antennas and Propagation Society International Symposium**. Orlando, FL, USA.
- _____ and R. Mittra. 2000. **Frontiers in Electromagnetics**. IEEE Press, New York.
- _____, K.C. Anusko and P.L. Werner. 1999. The Generation of Sum and Difference Patterns Using Fractal SubArrays. **Microwave And Optical Technology Letters**, 22: 524-526.

Wener, D. H., R. L. Haupt and P. L. Werner. 1999. Fractal Antenna Engineering: The Theory and Design of Fractal Antenna Arrays. **IEEE Antennas and Propagation Magazine**, 41: 37-59.

_____, W. Kuhirun and P. L. Werner. 2004. Fractile Arrays: A New Class of Tiled Arrays With Fractal Boundaries. **IEEE Transactions on Antennas and Propagation**, 52: 2008-2018.

_____, _____, _____ 2005. The Peano-Gosper Fractal Array. **IEEE Transactions on Antennas and Propagation**, 51: 2063-2072.

Yan, K. and Lu Y. 1997. Sidelobe Reduction in Array-Pattern Synthesis Using Genetic Algorithm. **IEEE Transactions on Antennas and Propagation**, 45: 1117-1122.

Zhu, J., A Hoorfar and N. Engheta. 2004. Peano Antennas. **IEEE Antennas and Wireless Propagation Letters**, 3: 71-74.

CURRICULUM VITAE

NAME : Mr. Songkran PISANUPOJ

BIRTH DATE : April 13, 1982

BIRTH PLACE : Bangkok, Thailand

EDUCATION	: <u>YEAR</u>	<u>INSTITUTE</u>	<u>DEGREE/DIPLOMA</u>
	2002	Kasetsart University	B.Eng. (Electrical)

POSITION/TITLE : Engineer

WORK PLACE : Provincial Electricity Authority